Quinone reduction by organo-osmium half-sandwich transfer hydrogenation catalysts

Bolitho, Elizabeth M.; Worby, Nathan G.; Coverdale, James; Wolny, Juliusz A.; Schunemann, Volker; Sadler, Peter J.

DOI:
10.1021/acs.organomet.1c00358

Document Version
Publisher's PDF, also known as Version of record

Citation for published version (Harvard):
Bolitho, EM, Worby, NG, Coverdale, J, Wolny, JA, Schunemann, V & Sadler, PJ 2021, 'Quinone reduction by organo-osmium half-sandwich transfer hydrogenation catalysts', *Organometallics*, vol. 40, no. 17, pp. 3012-3023. https://doi.org/10.1021/acs.organomet.1c00358

ORGANOMETALLICS

pubs.acs.org/Organometallics

Article

Quinone Reduction by Organo-Osmium Half-Sandwich Transfer Hydrogenation Catalysts

Elizabeth M. Bolitho, Nathan G. Worby, James P. C. Coverdale, Juliusz A. Wolny, Volker Schünemann, and Peter J. Sadler*

Cite This: https://doi.org/10.1021/acs.organomet.1c00358

Read Online

ACCESS | Metrics & More | Article Recommendations | Supporting Information

ABSTRACT: Organo-osmium(II) 16-electron complexes [$Os^{II}(\eta^6$-arene)(R-PhDPEN)] (where η^6-arene = *para*-cymene or biphenyl) can catalyze the reduction of prochiral ketones to optically pure alcohols in the presence of a hydride source. Such complexes can achieve the conversion of pyruvate to unnatural D-lactate in cancer cells. To improve the catalytic performance of these osmium complexes, we have introduced electron-donor and electron-acceptor substituents (R) into the *para* (R_1) or *meta* (R_2) positions of the chiral R-phenyl-sulfonyl-diphenylethyl-enediamine (R-PhDPEN) ligands and explored the reduction of quinones, potential biological substrates, which play a major role in cellular electron transfer chains. We show that the series of [$Os^{II}(\eta^6$-arene)(R-PhDPEN)] derivatives exhibit high turnover frequencies, enantioselectivities (>92%), and conversions (>93%) for the asymmetric transfer hydrogenation (ATH) of acetophenone-derived substrates and reduce duroquinone and menadione to their di-alcohol derivatives. Modeling of the catalysis using density functional theory (DFT) calculations suggests a mechanism involving formic acid deprotonation assisted by the catalyst amine groups, phenyl-duroquinone stacking, hydride transfer to Os^{II}, possible CO_2 coordination, and tilting of the η^6-arene ring, followed by hydride transfer to the quinone. These findings not only reveal subtle differences between Ru(II) and Os(II) catalysts, but also introduce potential biological applications.

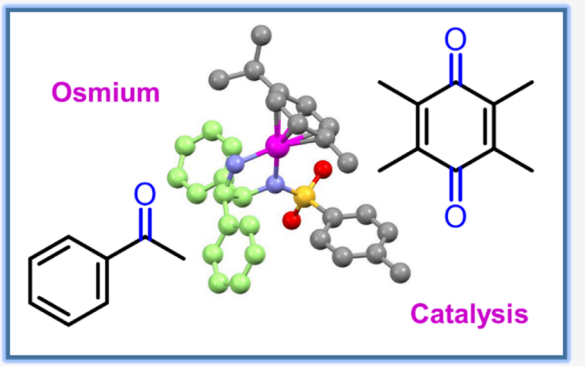

INTRODUCTION

Asymmetric transfer hydrogenation (ATH) involves metal-mediated catalytic transfer of hydride to a prochiral substrate (i.e., ketone or imine) in an enantioselective manner, to form a chiral product. This is of much industrial interest owing to the importance of optically active alcohols and amines in both agrochemicals and pharmaceuticals. For example, acetophenone is an industrial substrate which undergoes ATH enantioselectively to form (*S*) or (*R*)-1-phenylethanol, which are used as chiral precursors for a variety of applications including drugs, preservatives, fragrances, flavors, and cosmetics.[1] ATH catalysts are widely used in drug synthesis, while enzymatically catalyzed enantioselective reductions are crucial in many steps of cell metabolism.[2]

In 2001, Noyori et al. developed chiral ruthenium complexes with the general formula [Ru^{II}(diphosphane)(diamine)Cl_2] which catalyze the ATH of aldehydes, ketones, and imines with impressive enantiomeric excesses (*ee*) of 97−99%.[3−8] The enantioselectivity of such catalysts is controlled by the chirality of the phosphine group (i.e., BINAP) and the sterics of the incoming ketone/imine. Second-generation Ru^{II} half-sandwich catalysts with the general formula, [$Ru^{II}(\eta^6$-*p*-cym)(Ph-DPEN)], (where *p*-cym = *para*-cymene and Ph-DPEN = phenyl diphenylethylenediamine) are readily synthesized by reacting Ph-DPEN, 2-propanol, and [$RuCl_2(\eta^6$-arene)$]_2$ dimer under atmospheric conditions and exhibit high enantioselectivities (99%) and conversions (98%) for the reduction of ketones and imines.[9−19] In this case, the enantioselectivity is controlled by the phenyl groups of the chiral-chelated DPEN ligand, allowing selective reduction of ketones/imines through a six-membered pericyclic transition state (TS).[16,20]

In 2015, we reported a series of remarkably stable, easy-to-synthesize 16-electron osmium(II) complexes, analogous to the second-generation Noyori catalysts, with the general formula [$Os^{II}(\eta^6$-*p*-cym)(Ph-DPEN)] (Figure 1).[21] These complexes exhibit high catalytic activity for ATH of acetophenone-derived substrates (99% *ee* and 99% conversion) compared to analogous Ru(II) catalysts and do not require chemical activation prior to catalysis.[20]

Received: June 15, 2021

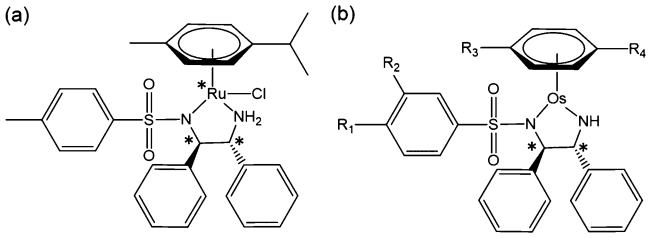

Figure 1. (a) Structure of Noyori's second-generation 18-electron half-sandwich ruthenium(II) pre-catalyst [$Ru^{II}(\eta^6$-*p*-cym)((1*R*,2*R*)-TsDPEN(H))Cl] (**Ru-1**). (b) General structure of coordinatively unsaturated 16-electron osmium(II) catalysts [$Os^{II}(\eta^6$-arene)-((1*R*,2*R*)(R-PhDPEN))] **1—16** (for R substituents see Table 1). * Denotes chiral centers.

Complex **1**, [$Os^{II}(\eta^6$-*p*-cym)TsDPEN] (where TsDPEN = tosyl diphenylethylenediamine), can also catalyze reductions in cancer cells, a possible basis for the design of anticancer agents with novel mechanisms of action.[20] Both the (1*S*,2*S*) and (1*R*,2*R*) isomers of **1** exhibit moderate *in vitro* anticancer activity against a panel of human cancer cell lines,[20,22,23] the potency of which can be drastically improved upon co-administration with non-toxic concentrations of sodium formate (an approved food additive) as the hydride source. Moreover, **1** was the first reported Os(II) synthetic catalyst to convert pyruvate (a metabolic substrate) enantioselectively to unnatural D-lactate and was specific for cancer versus healthy cells. This is significant, as cancer cells have elevated levels of lactate, thus making their metabolism a viable therapeutic target. Confocal microscopy studies of a fluorescently labeled derivative of **1** revealed that this family of complexes can also generate toxic reactive oxygen species (ROS) *in vivo*, which may allow exploitation of the redox vulnerabilities of cancer cells. Additionally, we have used synchrotron-XRF and ICP—MS to demonstrate that lysosomes and biological thiols (e.g., glutathione and cysteine) can play crucial roles in catalyst deactivation inside cells.[23] We also showed that such complexes are partially accumulated into cells by active (energy-dependent) mechanisms and remain intact in the cytosol where catalysis likely occurs.[23]

In addition to the catalytic reduction of pyruvate, it is relevant to explore other potential biological substrates present in the cytosol or cell organelles to focus on identifying new intracellular targets and to improve catalytic performance. In particular, quinones play major roles in electron transport in mitochondria, reactions which may contribute to a catalytic mechanism leading to cell death. Quinones can protect cells through various pathways, including modification of redox homeostasis, anti-inflammatory activities, or release of detoxification enzymes.[24] Notably, the two-electron reduction of quinones is known to be a major detoxification mechanism for most quinones;[25] hence, investigation of quinones as substrates for catalysis is of significant interest. The cofactor vitamin K_1 (phylloquinone) undergoes intracellular redox chemistry *via* its reduction (by nicotinamide adenine dinucleotide, NADH) or epoxidation, essential reactions in blood coagulation, and cell proliferation.[26] The derivative vitamin K_3 (menadione) has shown promising tumor-killing properties.[27] Menadione causes intracellular oxidation *via* the production of ROS disturbing the intracellular redox balance (oxidative stress-induced cytotoxicity).[27,28]

Here, we report the synthesis and characterization of a series of novel 16-electron Os^{II} half-sandwich complexes (**1—16**) with the general formula [$Os(\eta^6$-arene)(R-PhDPEN)] (arene = *p*-cymene or biphenyl, R-PhDPEN = R-substituted phenyl diphenylethylenediamine, Figure 1). Initially, the catalytic activity of these complexes in the reduction of acetophenone (a widely used screening candidate for ATH) was investigated

Table 1. Catalytic Conversion (%), Enantiomeric Excess (*ee*, %), and Turnover Frequency (TOF, h^{-1}) for the Reduction of Acetophenone to (*S*)- or (*R*)-1-phenylethanol by Os^{II} Complexes 1—16 in Comparison with Ru^{II} Complex Ru-1 in the Presence of 5:2 Formic Acid/Triethylamine Azeotrope for 24 h at 310 K as Determined by ^{1}H NMR and Chiral GC[a]

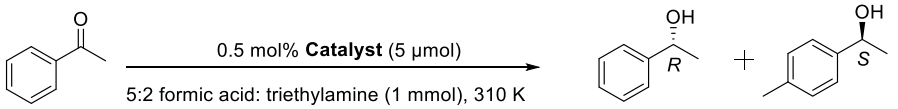

complex	catalyst chirality	R_1	R_2	R_3	R_4	conv. (%)[c]	config.	*ee*[d]	TOF (h^{-1})[c]
Ru-1	*SS*	CH_3	H	n/a	n/a	98	*S*	99	23 ± 1
1[b]	*RR*	CH_3	H	CH_3	^{i}Pr	99	*R*	99	63.6 ± 0.6
2[b]	*RR*	H	CH_3	CH_3	^{i}Pr	99	*R*	99	61.7 ± 0.6
3	*RR*	CF_3	H	CH_3	^{i}Pr	99	*R*	95	69.3 ± 0.7
4	*RR*	H	CF_3	CH_3	^{i}Pr	99	*R*	96	84.8 ± 0.8
5	*RR*	^{t}Bu	H	CH_3	^{i}Pr	98	*R*	98	105.5 ± 0.9
6[b]	*RR*	F	H	CH_3	^{i}Pr	99	*R*	96	40 ± 1
7[b]	*RR*	Br	H	CH_3	^{i}Pr	99	*R*	97	81 ± 2
8[b]	*SS*	I	H	CH_3	^{i}Pr	97	*S*	95	85 ± 5
9[b]	*RR*	CH_3	H	H	Ph	98	*R*	92	78.2 ± 0.4
10[b]	*RR*	H	CH_3	H	Ph	98	*R*	97	71.5 ± 0.7
11	*SS*	CF_3	H	H	Ph	99	*S*	95	70.4 ± 0.6
12	*SS*	H	CF_3	H	Ph	98	*S*	99	82.8 ± 0.8
13	*RR*	^{t}Bu	H	H	Ph	99	*R*	98	125.1 ± 0.8
14	*RR*	F	H	H	Ph	98	*R*	95	92.6 ± 0.9
15	*RR*	Br	H	H	Ph	99	*R*	95	92.8 ± 0.8
16	*SS*	I	H	H	Ph	98	*S*	99	95.7 ± 0.8

[a] *ee* were determined in triplicate and were within ±0.5%. [b] Previously reported data.[21,23] [c] Determined by ^{1}H NMR. [d] Determined by chiral GC.

https://doi.org/10.1021/acs.organomet.1c00358
Organometallics XXXX, XXX, XXX−XXX

Table 2. Catalytic Conversion (%), *ee* (%), and TOF (h^{-1}) for the Reduction of 2-Chloroacetophenone or 4-Methoxyacetophenone Using *RR*-Configured catalysts 1, 5, 13, and 16 in the Presence of 5:2 Formic Acid/TEA Azeotrope for 24 h at 310 K as Determined by ^{1}H NMR and Chiral GC

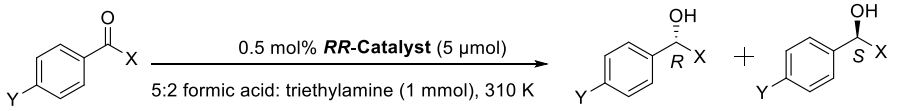

X	Y	catalyst	S/C[a]	conv. (%)[b]	config.	*ee* (%)[c]	TOF (h^{-1})[b]
CH_2Cl	H	**1**	100	97	*S*	94	n.d.
CH_2Cl	H	**5**	100	99	*S*	98	111.0 ± 0.6
CH_2Cl	H	**13**	100	99	*S*	98	138.8 ± 0.8
CH_3	OCH_3	**1**	100	67	*R*	n.d.	n.d.
CH_3	OCH_3	**5**	100	70	*R*	98	34.4 ± 0.5
CH_3	OCH_3	**13**	100	88	*R*	99	53.2 ± 0.9

[a]S/C = substrate/catalyst mol ratio. [b]Determined by ^{1}H NMR. [c]Determined by chiral GC.

and later applied in a biological context to two quinones (duraquinone and menadione) to further probe the potential scope for their catalytic activity inside cancer cells. Density Functional Theory (DFT) calculations suggest that the mechanism of catalytic reduction of quinones by such catalysts with formate as the hydride donor may have some unusual features.

RESULTS AND DISCUSSION

Synthesis and Characterization. We introduced various substituents (R) into chiral *R*-phenyl-sulfonyl-diphenylethylenediamine (Ph-DPEN) ligands by coupling phenylsulfonyl chlorides carrying electron donors CH_3 or ^{t}Bu or electron acceptors CF_3, F, Br, or I in *para* (R_1) or *meta* (R_2) positions for (1*S*,2*S*) or (1*R*,2*R*)-diphenylethylenediamine (DPEN) using a reported method.[29] All ligands (**L1**−**L4**) were recrystallized from hot ethyl acetate, characterized by ^{1}H and ^{13}C NMR, HR-MS with purity >95% assessed by CHN analysis. The new ligands were then reacted with $[Os(\eta^6\text{-}p\text{-cymene})Cl_2]_2$ or $[Os(\eta^6\text{-biphenyl})Cl_2]_2$ dimers (synthesized using reported methods),[21,30] *via* a previously reported biphasic reaction,[21] in the presence of a base to generate enantiomerically pure half-sandwich complexes **1**−**16** (Table 1). All Os^{II} complexes (**1**−**16**) were characterized by ^{1}H and ^{13}C NMR, UV−visible spectroscopy, and HR-MS and CHN analyses, all with >95% purity.

Catalytic Reduction of Acetophenone Derivatives. The effect on the catalytic activity of the phenylsulfonyl ring electron-donor or electron-acceptor substituents was investigated. Initially, we assessed the ATH catalytic activity of **1**−**16** toward acetophenone in the presence of formic acid as a hydride source, as determined by both ^{1}H NMR spectroscopy and gas chromatography−flame-ionization detection (GC−FID) (Table 1). The time dependence of the catalytic reactions was monitored by ^{1}H NMR. The catalytic turnover frequency (TOF) (h^{-1}) was determined from ^{1}H NMR spectra by monitoring the decrease in intensity of the singlet of acetophenone (2.10 ppm) and the formation of the quartet for 1-phenylethanol (4.75 ppm). Acetophenone is prochiral, and the chirality of the 1-phenylethanol product was determined by chiral gas chromatography (GC) against known retention times for the (*S*) or (*R*) alcohol products. Complexes **1**−**16** all achieved high catalytic conversion (>98%) and *ee* (>92%) for this reduction, exhibiting maximum turnover frequencies of >61 h^{-1}, which is ca. 3× faster than that of Noyori's ruthenium catalyst (23 ± 1 h^{-1}).[21] Interestingly, the catalytic activity of complexes with biphenyl as the arene was significantly higher for the enantioselective reduction of acetophenone compared to the analogous Os^{II} *p*-cymene complexes (2.3× faster for fluorine complex **14** versus **6**, Table 1).

Catalysts bearing ^{t}Bu groups at the *para* (R_1, Figure 1) positions (**5** and **13**, *p*-cymene and biphenyl, respectively) exhibited higher catalytic turnover frequencies (TOF = 105.5 ± 0.9 and 125.1 ± 0.8 h^{-1}) for the enantioselective reduction of acetophenone. Remarkably, these reactions were faster than for the parent compounds $[Os^{II}(\eta^6\text{-}p\text{-cym})(TsDPEN)]$ (**1**, 63.6 ± 0.6 h^{-1}) and $[Os^{II}(\eta^6\text{-biph})(Ph\text{-}DPEN)]$ (**9**, 78.2 ± 0.4 h^{-1}) and >5× faster than that of Noyori's ruthenium catalyst (23 ± 1 h^{-1}), while maintaining high enantioselectivity (98%) and conversions (99%). The bulky electron-donating *tert*-butyl groups of **5** and **13** may hinder the rotation of the large electron-withdrawing arene groups, stabilizing the pericyclic transition state resulting in faster ATH.[21,31−33]

Moving the substituent position from *para* (R_1) to *meta* (R_2) on the PhDPEN ligand influenced the catalytic activity. Comparison of *p*-cymene complexes **3** (*p*-CF_3) and **4** (*m*-CF_3) revealed that **3** (69.3 ± 0.7 h^{-1}) catalyzed the reduction of acetophenone at a significantly slower rate compared to **4** (84.8 ± 0.8 h^{-1}). The same trend was observed for the biphenyl *p*-CF_3 and *m*-CF_3 analogues (**11** and **12**, respectively). This may imply that strongly electron-withdrawing groups at the *meta* position stabilize a partial negative charge on the adjacent carbon, enhancing the acidity of the osmium center. In contrast, the *p*-CH_3 and *m*-CH_3 *p*-cymene analogues (**1** and **2**) give rise to no change in the catalytic activity (p = 0.0179); however, a small increase in TOF was observed for the biphenyl analogues **9** (78.2 ± 0.4 h^{-1}) and **10** (71.5 ± 0.7 h^{-1}). This is perhaps due to enhanced steric repulsion from the *meta*-CH_3 and the bulky biphenyl group, amplified in **10** versus **9**.[34]

To explore the substrate diversity of *tert*-butyl complexes **5** and **13** (the most promising for acetophenone reduction), we also screened their catalytic potential against acetophenone derivatives 2-chloroacetophenone and 4-methoxyacetophenone (Table 2). The TOFs and conversion of 2-chloroacetophenone to 2-chloro-1-phenylethan-1-ol were determined by comparing the relative ^{1}H NMR integrals of the product doublet (CH_2Cl, 3.35 ppm) and diminishing reagent doublet (*o*-Ar*H*, 7.57 ppm), Supporting Information, Figure S2. Similarly, the reduction of 4-methoxyacetophenone to 1-(4-methoxyphenyl)ethan-1-ol was monitored by the ^{1}H NMR product quartet (C*H*OH, 4.37 ppm) and the reduction

https://doi.org/10.1021/acs.organomet.1c00358
Organometallics XXXX, XXX, XXX−XXX

Table 3. Catalytic Conversion (%), and TOF for Reduction of (a) Duroquinone and (b) Menadione Using Catalysts 1, 5, 13, and 16 in the Presence of 5:2 Formic Acid/TEA Azeotrope for 12 h at 310 K as Determined by ^{1}H NMR

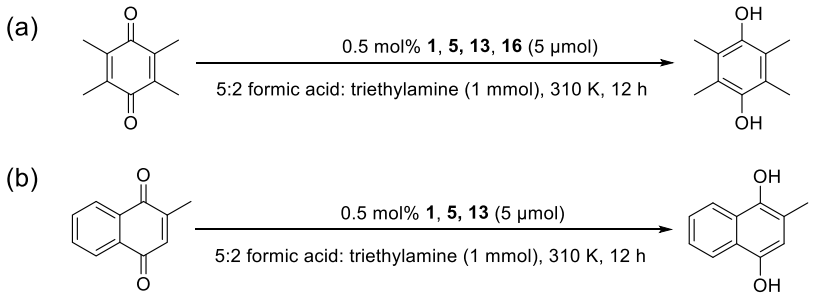

	catalyst	S/C	conv. (%)	TOF (h^{-1})
duroquinone (a)	**1**	200	98	48.1 ± 0.4
	5	200	99	67.9 ± 0.6
	13	200	97	55.5 ± 0.3
	16	200	92	36.5 ± 0.5
menadione (b)	**5**	200	87	94 ± 2
	13	200	96	145 ± 3

of the reagent singlet (CH_3, 2.03 ppm, Supporting Information, Figure S3).

tert-Butyl complexes **5** (arene = *p*-cym) and **13** (arene = biph) were shown to catalyze the reduction of 2-chloroacetophenone to the corresponding *S*-configured alcohol with high conversion (99%), *ee* (98%), and TOF (111.0 ± 0.6 and 138.8 ± 0.8 h^{-1}). In contrast, the reduction of 4-methoxyacetophenone by **5** and **13** revealed lower percentage conversions (70 and 88%, respectively) and TOF (34.4 ± 0.5 and 53.2 ± 0.9 h^{-1}), but still maintained higher *ee* (98 and 99%) under the same conditions. A higher catalytic turnover for both substrates was observed for biphenyl complex **13** compared to the *p*-cymene analogue **5** (the same trend observed for acetophenone itself), likely owing to the increased electron-withdrawing properties of biphenyl.

Catalytic Reduction of Quinones. This family of organo-osmium catalysts exhibits enhanced anticancer activity *in vitro* when a hydride source is added,[20,23] and can convert cellular pyruvate to unnatural D-lactate, leading to cell death.[20] However, catalytic turnover for this reaction inside cells was extremely low,[20] which is partially attributable to in-cell deactivation of the catalyst (e.g., by thiols and lysosomes) in the cytosol,[23] but perhaps other cellular molecules can also act as substrates. Understanding the intracellular catalytic activity of these complexes may be crucial for their progression toward preclinical development. Therefore, we have investigated the possibility that quinones are potential substrates for ATH.

Quinones are highly redox-active and are capable of cycling with their semiquinone radical anions, allowing the generation of toxic ROS,[35] perturbing cellular redox homeostasis through the oxidation of biomolecules (such as lipids, proteins, and DNA).[24] To further explore the versatility of organo-osmium complexes toward biological substrates and possible in-cell catalysis, we have screened our most active catalysts for their ability to reduce quinones in the presence of formic acid.

The ability of this family of complexes to catalyze the reduction of the quinones, duroquinone and menadione, was investigated using the three most promising osmium catalysts (**5**, **13**, and **16**), in addition to parent compound **1**. The catalytic reduction of duroquinone and menadione in the presence of 5:2 formic acid/TEA azeotrope was monitored, and the reduction products for each quinone substrate were characterized by nuclear magnetic resonance (NMR) (^{1}H, ^{13}C, ^{1}H COSY, ^{1}H−^{13}C HSQC, ^{1}H−^{13}C HMQC) and ESI-MS.

The reduction of duroquinone in the presence of *tert*-butyl complex **5** and formic acid was monitored over 24 h, and the identity of the product was investigated (Supporting Information, Figure S4). The color of the solution changed from light to dark yellow instantly, and after 24 h, it was brown. The sharp ^{1}H NMR signals confirmed the formation of durohydroquinone, the fully reduced aromatic dialcohol (Supporting Information, Figures S4). Notably, the four equivalent methyl groups (CH_3) were downfield shifted from 1.95 to 2.06 ppm and the reduction of both ketone groups to alcohols (7.33 ppm, O*H*) was observed. The DEPT ^{13}C NMR spectrum further confirmed the structures, displaying three carbon environments: 146.1, 121.8, and 13.4 ppm (Supporting Information, Figure S5). The disappearance of the strongly deshielded carbonyl carbons of duroquinone (187.2 ppm) and appearance of the aromatic alcohols (121.8 ppm) confirmed the formation of durohydroquinone. ^{1}H−^{13}C HSQC and HMBC NMR (Supporting Information, Figures S6 and S7) and ESI-MS (*m*/*z* calcd for $C_{15}H_{17}O_2N_2$ $[M + 2Na-H]^+$, 211.1; found: 211.3) also supported this assignment. As all NMR spectra were highly resolved, it is likely that any paramagnetic intermediates were short-lived during the catalytic conversions.

Next, the TOF and percentage conversion of duroquinone to durohydroquinone were determined using ^{1}H NMR by comparing the relative integrals of the newly formed durohydroquinone singlet (CH_3, 1.74 ppm) and diminishing duroquinone singlet (CH_3, 1.44 ppm), Supporting Information, Figure S8. The O*H* peak for the product (7.33 ppm) was not integrated due to exchange broadening. All three of the complexes analyzed (**1**, **5**, **13**) demonstrated high conversions (>92%) and TOFs (>36 h^{-1}, substrate/catalyst molar ratio = 200) for duroquinone. Unlike the ATH of aromatic ketones, the *p*-cymene complex **5** (67.9 ± 0.6 h^{-1}) catalyzed the reduction of duroquinone faster than that of the biphenyl analogue **13** (55.5 ± 0.3 h^{-1}) and parent compound **1** (48.1 ± 0.4 h^{-1}). Duroquinone is a highly conjugated planar substrate with steric hindrance around both keto groups (two adjacent methyl groups). Substrate steric bulk may disfavor the transition state for reduction, and thus, complexes with an

https://doi.org/10.1021/acs.organomet.1c00358
Organometallics XXXX, XXX, XXX−XXX

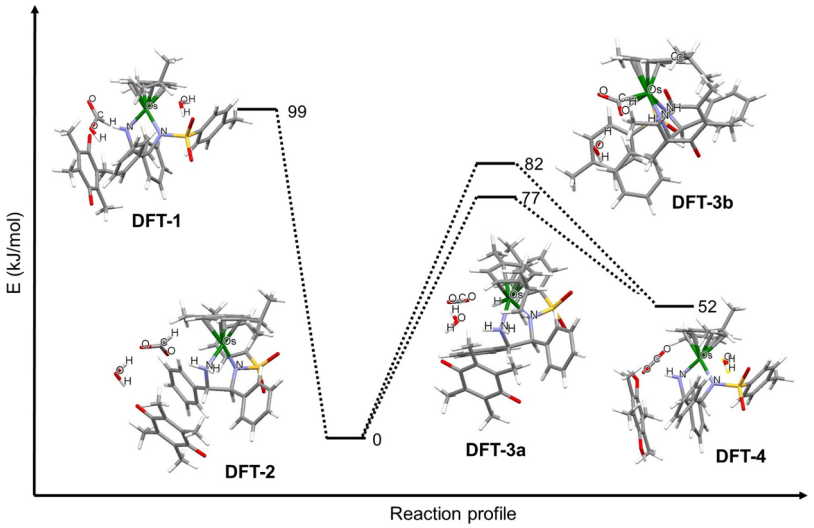

Figure 2. DFT energy reaction coordinate describing the pathway for the catalytic reduction of duroquinone to durohydroquinone in the presence of **1** and formic acid.

extended η^6-arene (biphenyl) may further obstruct the substrate approach.

A similar NMR approach was used to confirm the product formed when menadione reacts with osmium catalysts **5** or **13** in the presence of formic acid for 24 h (Supporting Information, Figure S9). The light-yellow menadione solution immediately darkened (2 min) and after 24 h appeared black, which on extraction gave rise to bright purple needle-like crystals. This correlates with the crystalline purple appearance of menadiol reported in the literature,[36] suggesting that menadione undergoes reduction to its aromatic diol (ESI-MS: *m*/*z* calcd for $C_{15}H_{17}O_2N_2$ $[M + 2ACN + H]^+$, 257.1, found: 257.2). Distinctive changes in the ^{1}H NMR spectrum corresponded to menadiol formation with the expected chemical environments (Supporting Information, Figure S9). The two peaks for strongly deshielded non-equivalent alcohol substituents at 9.39 (*H*OCCH) and 8.29 ppm (*H*OCCH$_3$), correlated to the adjacent C−H carbon (111.8 ppm) and CH$_3$ carbon (17.0 ppm), respectively in the ^{1}H−^{13}C HMBC spectrum (Supporting Information, Figure S10). The O*H* proton at 8.29 ppm is shielded by the adjacent electron-donating CH$_3$ group. Furthermore, the CH$_3$ group (2.31 ppm) and neighboring downfield C*H* group (^{1}H 6.66 ppm, ^{13}C 111.8 ppm) correlated strongly in both COSY and HMBC spectra (Supporting Information, Figure S11 and S12).

All ^{1}H and ^{13}C NMR assignments were confirmed in the 2D ^{1}H−^{13}C HSQC spectrum (Supporting Information, Figure S12). Menadiol formation likely proceeds *via* the semiquinone intermediate, favorably gaining aromaticity driven by the additional stabilization from extended conjugation *via* resonance with the fused phenyl ring. The percentage conversions and TOFs for the reduction of menadione to menadiol by *tert*-butyl complexes **5** and **13** were determined by comparing the relative ^{1}H NMR integrals of the menadiol singlet (C*H*$_3$, 2.44 ppm) and diminishing menadione singlet (C*H*$_3$, 2.10 ppm), Supporting Information, Figure S13. Both **5** and **13** exhibited high conversions (>87%) and TOFs (>94 ± 2 h^{-1}) for the reduction of menadione (Table 3). Interestingly, the biphenyl complex (**13**) catalyzed the reaction more efficiently than the *p*-cymene analogue (**5**), with TOFs of 145 ± 3 and 94 ± 2 h^{-1}, respectively. Unlike duroquinone, one of the carbonyls in menadione is less sterically hindered (no adjacent CH$_3$ group), thus is more susceptible to nucleophilic attack. This exposed carbonyl could drive the initial reduction *via* the semi-quinone intermediate (gaining aromaticity), increasing the energetic favorability of forming the fully reduced product (second reduction).

This appears to be the first example of the reduction of quinones by synthetic half-sandwich osmium(II) complexes and may have implications for transfer hydrogenation reaction in cells. The reduction of menadione results in increased oxidative stress in cells by redox cycling and the generation of ROS, which can lead to cell death—particularly for cancer cells which survive and proliferative under extreme conditions. For example, ascorbate can induce oxidative stress which kills breast cancer cells *via* the in-cell reduction of menadione.[37] The ability for **1** to reduce menadione is consistent with the reported generation of ROS in cells and in zebrafish embryos.[22] Hence, translation of this work into a biological context may allow identification of further biomolecules involved in the anticancer mechanism(s) of action. Likewise, duroquinone allows the regeneration of quinone reductases in cells and can raise the NAD$^+$/NADH ratio, which helps cells to survive in low NAD$^+$ conditions,[38,39] thus promoting cell survival. Interestingly, this complements the ability of **1** to catalytically convert 1,4-NADH to NAD$^+$.[40] Optimization of such catalysts under biologically relevant conditions may give rise to the identification of new substrates, providing further insights into the catalytic mechanism(s) of action in cancer cells.

DFT Modeling of Quinone Catalysis. In order to elucidate the mechanism for the catalytic reduction of duroquinone in the presence of complex **1** and formic acid, DFT calculations were performed (Figure 2). DFT is a valuable tool in bioinorganic chemistry which can be used to model the structure and properties of complexes by providing a solution obtained upon minimization of the density functional.[41]

At the start of the reaction, the calculations show the catalyst, quinone substrate (duroquinone), formic acid (HCOOH), and water (**DFT-1**, Figure 2, see also pdb file 1.pdb in Supporting Information) with duroquinone parallel to

https://doi.org/10.1021/acs.organomet.1c00358
Organometallics XXXX, XXX, XXX−XXX

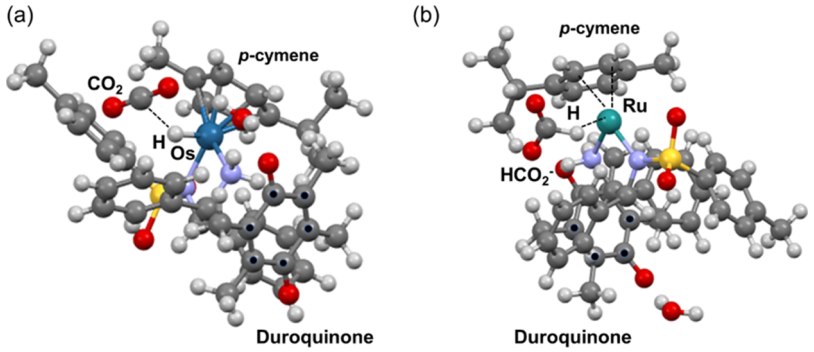

Figure 3. DFT structures for the catalytic reduction of duroquinone in the presence of ***SS*-1** (Os) or ***SS*-Ru-1** and formic acid. (a) Intermediate **3a** (Figure 2, 77 kJ/mol) showing an Os−H bond (1.608 Å) is formed, while linear CO_2 remains in the second coordination sphere forming a T-shaped contact with the hydride and a C−H bond length of 2.46 Å. The η^6-coordination of the arene is retained. (b) Optimized structure of ***SS*-Ru-1** showing Ru−HCO_2^- coordination *via* a Ru−H bond of distance 1.72 Å. Note that the optimized structure of the Ru complex corresponds to a different diasteroisomer (the absolute configuration of the *N*,*N*′ ligand is retained, yet the absolute configuration of the metal center is different). Atom colors: H light gray; C dark gray; N violet; O red; S, yellow; Ru teal; Os dark cyan. Some C atoms of the duroquinone ring are labeled with black dots to aid identification.

one of the phenyl groups of DPEN with an onset of (two C−C contacts of 3.68 and 3.60 Å) stacking interactions. Interestingly, the O-atoms of formic acid point away from the osmium catalyst, and instead, it is orientated with its H-atom toward the Os^{II} center with an H−Os distance of 3.05 Å. As the reaction proceeds, formate is deprotonated by transferring H^+ to the NH group of the catalyst (**DFT-2**, Figure 2, file 2.pdb in Supporting Information), with the water molecule now in close proximity to formate. In the structure of **DFT-2**, duroquinone is still roughly parallel to the phenyl group of DPEN, with previously mentioned C−C contacts of 3.72 and 3.45 Å, respectively. As the reaction proceeds further, two intermediates are formed, **DFT-3a** and **DFT-3b** (Figure 2), with the former being lower in energy. In intermediate **DFT-3a** (77 kJ/mol, see the file 3a.pdb in Supporting Information) an Os−H bond (1.608 Å) is formed (Figure 3). The CO_2 molecule stays in the second coordination sphere, forming a T-shaped contact with the hydride with a C−H distance of 2.46 Å (Figure 3). The η^6-coordination of the arene is retained (Figure 3). Alternatively, in the intermediate **DFT-3b** (Figure 2) (82 kJ/mol, see file 3b.pdb in Supporting Information), both bent CO_2 (O−C−O angle of 124.6°) and hydride (H^-) are bound to the osmium center with bond distances of 2.206 and 1.580 Å, respectively. This causes a weakening of the arene coordination, with a mean Os−C distance of 2.464 Å compared to 2.397 Å for the second hydride complex, a greater elongation of two of the Os−C bonds by ca. 0.2 Å. The consequent ring-tilt in the coordinated η^6-arene of the *para*-cymene allows the duroquinone to approach on the opposite side to the reactive Os−H bond (Figure 2). In this structure, the duroquinone is no longer parallel to the phenyl groups of DPEN. It is notable that we were unable to optimize any structure with the HCO_2^- bound to osmium. However, for the Ru analogue, Ru−HCO_2^- coordination was found with a Ru−H distance of 1.72 Å (Figure 3). Finally, the quinone accepts hydride from Os−H and a proton from solution, to reduce both C═O groups of the duroquinone substrate to form durohydroquinone (**DFT-4**, Figure 2, see file 4b.pdb in Supporting Information). The osmium catalyst **1** is regenerated in the process.

EXPERIMENTAL SECTION

Chemical Reagents. Osmium trichloride ($OsCl_3 \cdot 3H_2O$) was the kind gift of Heraeus. (1*R*,2*R*) and (1*S*,2*S*)-1,2-diphenylethylenediamine were purchased from Alfa Aesar, respectively. All benzenesulfonyl chlorides, acetophenone, 2-chloroacetophenone, 4-methoxyacetophenone, duroquinone, 5:2 formic acid triethylamine azeotrope, *β*-nicotinamide adenine dinucleotide (disodium salt), anhydrous magnesium sulfate, and anhydrous dichloromethane were purchased from Sigma-Aldrich (UK), along with all deuterated solvents: d_6-benzene, *d*-chloroform, and DMSO-d_6. All commercial solvents were purchased from Sigma-Aldrich (UK).

Electrospray Ionization Mass Spectrometry. Ligands and complexes were dissolved in the minimum amount of DCM and diluted in acetonitrile and analyzed on a high-resolution Bruker maXis II Q-TOF mass spectrometer (electrospray in positive mode) with a scan range of m/z 50−3000 (1 Hz spectra rate). The quinone reduction products were dissolved in acetonitrile and analyzed on a low-resolution single quad Agilent 6130B (electrospray in positive mode) with a scan range of either m/z 400−1000 or m/z 50−500.

Elemental Analysis. Carbon, hydrogen, and nitrogen (CHN) analyses was performed in duplicate by Warwick Analytical Services on an Exeter Elemental Analyser CE440.

Chiral Gas Chromatography. GC experiments were conducted using the GC−FID, CHROMPAC cyclodextrin-*β*-236M-19, 50 m × 0.25 mm × 0.25 *μ*m, P = 15 psi, H_2 gas, T = 473 K.

Microwave Reactor. For the synthesis of osmium dimers, a CEM Discovery SP Microwave Reactor was used in *p*-cymene and biphenyl dimer synthesis (10 min, 413 K, 200 W, and 250 psi), and biphenyl complex synthesis (10 min, 393 K, 150 W, and 250 psi).[21,23]

Nuclear Magnetic Resonance. Unless otherwise stated, all samples were prepared in DMSO-d_6 in 5 mm NMR tubes and recorded at 298 K using Bruker AVANCE III HD 500 MHz or Bruker AVANCE III HD 400 MHz (^{1}H) instruments. For kinetic studies, the Bruker AVANCE III HD 400 MHz was used to record spectra every 2−10 min at 310 K. Bruker TOPSPIN 3.0 and SpinWorks Java (2019) were utilized to process all data.

DFT Calculations. The relevant structures were optimized using the B3LYP exchange−correlation functional[42] and CEP-31g basis set[43] and Grimme D3 dispersion correction.[44] All calculations have been performed with Gaussian 16.[45] The Gaussians IEFPCM option was used to model the formic acid as solvent. The modeling was performed for the duroquinone reduction with the ***SS*-1** complex as the catalyst. The formation of the hydride complex introduces an additional chirality center on the osmium leading to diasteroisomerism. In our modeling, we considered only one diastereoisomer with the above given absolute configuration of the ligand. The structure of

https://doi.org/10.1021/acs.organomet.1c00358
Organometallics XXXX, XXX, XXX−XXX

the diasteroisomer is shown in the pdb files 3a.pdb and 3b.pdb in Supporting Information.

Synthesis and Characterization of Ligands. *General Synthesis of Benzenesulfonamide Ligands (**L1**–**L4**).* To a solution of (1*R*,2*R*)-1,2-diphenylethylenediamine or (1*S*,2*S*)-1,2-diphenylethylenediamine (1 mol equiv) and triethylamine (1 mol equiv) in anhydrous dichloromethane (50 mL) cooled in an ice bath, the chosen sulfonyl chloride (1.2 mol equiv) in anhydrous dichloromethane (150 mL) was added dropwise over 1 h. The ice bath was removed, and the reaction mixture was stirred for 5 h. The product was extracted with distilled water (3 × 10 mL), dried over magnesium sulfate, and concentrated *in vacuo* with diethyl ether to yield a solid.

*N-(2-Amino-1,2-diphenylethyl)-3-methylbenzenesulfonamide (**RR-L1**).* Synthesized as per the general procedure using (1*R*,2*R*)-1,2-diphenylethylenediamine (0.7 g, 3.20 mmol, 1 mol equiv), triethylamine (46 mL, 3.2 mmol, 1 mol equiv), and 3-methylbenzenesulfonyl chloride (0.464 mL, 3.2 mmol, 1 mol equiv). The product was recrystallized in hot ethyl acetate to yield a pale yellow amorphous solid (0.99 g, 2.95 mmol, 92.3%). ^{1}H NMR (500 MHz, DMSO-d_6, 298 K, TMS): δ 7.35–7.30 (m, 1H, SO_2ArH), 7.24–7.17 (m, 3H, SO_2ArH), 7.16–7.08 (m, 5H, ArH), 7.04–6.87 (m, 5H, ArH), 4.39 (d, ^3J(H,H) = 7.6 Hz, 1H, NHC*H*Ph), 4.00 (d, ^3J(H,H) = 7.6 Hz, 1H, NH_2CHPh), 2.19 (3*H*, CH_3ArSO_2); ^{13}C NMR (125 MHz, DMSO-d_6, 298 K): δ 142.5, 141.1, 139.5, 137.9, 132.2, 128.3, 127.5, 127.3, 126.6, 123.2, 64.9, 60.6, 20.6; HRMS (ESI): *m*/*z* calcd for $C_{21}H_{23}N_2O_2S$ [M + H]$^+$, 367.1480; found: 367.1476. Elemental analysis Calcd (%) for $C_{21}H_{22}N_2O_2S$: C, 68.87 (68.83); H, 6.09 (6.05); N, 7.69 (7.64).

*N-(2-Amino-1,2-diphenylethyl)-4-(trifluoromethyl)-benzenesulfonamide (**RR-L2**).* Synthesized as per the general procedure using (1*R*,2*R*) or (1*S*,2*S*)-1,2-diphenylethylenediamine (0.36 g, 1.69 mmol, 1 mol equiv), triethylamine (0.23 mL, 1.65 mmol, 1 mol equiv), and 4-(trifluoromethyl)benzene sulfonyl chloride (0.51 g, 2.07 mmol, 1.2 mol equiv). A white amorphous solid (0.306 g, 0.7267 mmol, 44.1%) was formed. ^{1}H NMR (500 MHz, DMSO-d_6, 298 K, TMS): δ 7.59–7.50 (m, 4H, ArH), 7.15–7.04 (m, 5H, ArH), 6.97–6.75 (m, 5H, ArH), 4.37 (d, ^3J(H,H) = 6.5 Hz, 1H, NHC*H*Ph), 3.98 (d, ^3J(H,H) = 6.5 Hz, 1H, NH_2CHPh); ^{13}C NMR (125 MHz, DMSO-d_6, 298 K, TMS): δ 145.4, 142.9, 139.8, 131.9, 131.6, 128.1, 127.9, 127.8, 127.7, 127.5, 127.1, 126.9, 126.1, 65.6, 61.0; HRMS (ESI): *m*/*z* calcd for $C_{21}H_{20}F_3N_2O_2S$ [M + H]$^+$, 421.1198; found, 421.1190. Elemental analysis Calcd (%) for $C_{21}H_{19}F_3N_2O_2S$: C, 60.00 (59.99); H 4.56 (4.56); N, 6.61 (6.66).

*N-(2-Amino-1,2-diphenylethyl)-3-(trifluoromethyl)-benzenesulfonamide (**RR-L3**).* Synthesized as per the general procedure using (1*R*,2*R*) or (1*S*,2*S*)-1,2-diphenylethylenediamine (0.73 g, 3.42 mmol, 1 mol equiv), triethylamine (0.48 mL, 3.41 mmol, 1 mol equiv), and 3-(trifluoromethyl)benzenesulfonyl chloride (0.655 mL, 4.09 mmol, 1.2 mol equiv). The product was recrystallized with hot ethyl acetate to yield a pale yellow crystalline solid (0.414 g, 0.984 mmol, 28.8%). ^{1}H NMR (500 MHz, DMSO-d_6, 298 K, TMS): δ 8.95–8.87 (m, 1H, NH_2), 7.83 (d, ^3J(H,H) = 8.0 Hz, 1H, $F_3CCHCHCH$), 7.79 (d, ^3J(H,H) = 8.5 Hz, 1H, $F_3CCHCHCH$), 7.66 (s, 1H, F_3CCHC), 7.57 (t, ^3J(H,H) = 7.5 Hz, 1H, $F_3CCHCHCH$), 7.33–7.25 (m, 5H, Ar*H*), 6.94–6.85 (m, 5H Ar*H*), 4.81 (d, ^3J(H,H) = 10.0 Hz, 1H, NHC*H*CH), 4.59 (d, ^3J(H,H) = 10.5 Hz, 1H, NHCHC*H*); ^{13}C NMR (125 MHz, DMSO-d_6, 298 K, TMS): δ 173.0, 142.1, 135.1, 134.1, 130.1, 128.3, 128.2, 127.7, 127.6, 122.9, 61.7, 58.1, 32.3; HRMS (ESI): *m*/*z* calcd for $C_{21}H_{20}F_3N_2O_2S$, [M + H]$^+$, 421.1198; found, 421.1196. Elemental analysis Calcd (%) for $C_{21}H_{19}F_3N_2O_2S$: C, 59.97 (59.99); H, 4.59 (4.63); N, 6.67 (6.63).

*N-2-Amino-1,2-diphenylethyl-4-(tert-butyl)benzenesulfonamide (**RR-L4**).* Synthesized as per the general procedure using (1*R*,2*R*)-1,2-diphenylethylenediamine (0.76 g, 3.58 mmol, 1 mol equiv), triethylamine (0.50 mL, 3.58 mmol, 1 mol equiv), and 4-(*tert*-butyl)benzenesulfonyl chloride (1.17 g, 5.01 mmol, 1.4 mol equiv). The product was recrystallized from hot ethyl acetate to yield a white solid amorphous solid (1.267 g, 3.10 mmol, 86.7%). ^{1}H NMR (500 MHz, DMSO-d_6, 298 K, TMS): δ 8.75 (s, 1H, NH_2) 7.31–7.27 (m, 2H, ArH), 7.24–7.14 (m, 7H, ArH), 6.86–6.75 (m, 5H, ArH), 4.63 (d, ^3J(H,H) = 9.5 Hz, 1H, NHC*H*Ph), 4.47 (d, 1H, ^3J(H,H) = 10.0 Hz, NH_2CHPh), 1.19 (s, 9H, Ar(CH_3)$_3$); ^{13}C NMR (125 MHz, DMSO-d_6, 298 K): δ 154.6, 137.6, 135.3, 134.2, 128.6, 128.2, 127.6, 127.5, 126.1, 125.1, 61.5, 58.4, 45.3, 30.7; HRMS (ESI): *m*/*z* calcd for $C_{24}H_{29}N_2O_2S$ [M + H]$^+$, 409.1871; found, 409.1875. Elemental analysis Calcd (%) for $C_{24}H_{28}N_2O_2S$: C, 70.58 (70.56); H, 6.94 (6.91); N, 6.90 (6.86).

Synthesis and Characterization of Complexes. Complexes **1**, **6**, **7**, **8**, and **9** were synthesized as previously reported.[20,23]

General Synthesis of Osmium p-Cymene Complexes. Osmium *p*-cymene-chlorido dimer ([Os(η^6-*p*-cym)Cl$_2$]$_2$, 1 mol equiv) was dissolved in DCM and benzenesulfonamide ligand (2.15 mol equiv) were stirred in DCM (15 mL). KOH (~50 mg) was added followed by water (to dissolve the base). A color change from yellow was observed upon vigorous stirring. The organic layer was concentrated *in vacuo* to typically yield a red-orange solid which was recrystallized from DCM/hexane.

*[Os(p-cym)(m–CH_3–BsDPEN)] (**2**).* Synthesized as per the general procedure using [Os(η^6-*p*-cymene)Cl$_2$]$_2$ (51.5 mg, 0.065 mmol, 1 mol equiv) and ***RR*-L1**, *N*-((1*R*,2*R*)-2-amino-1,2-diphenylethyl)-3-methylbenzenesulfonamide (47.6 mg, 0.13 mmol, 2 mol equiv). A rapid color change from a yellow to dark orange solution was observed in the bottom (organic) layer upon addition of KOH (56.1 mg, 1 mmol, 15 mol equiv). The solid was recrystallized from DCM/hexane to yield a dark brown amorphous solid (43.1 mg, 0.061 mmol, 93.8%). ^{1}H NMR (500 MHz, DMSO-d_6, 298 K, TMS): δ 8.16 (s, 1H, N*H*), 7.49 (d, 2H, ^3J(H,H) = 7.0 Hz, SO_2ArH), 7.30–7.07 (m, 11H, Ar*H*), 6.97–6.79 (m, 1H, Ar*H*), 5.87 (d, 1H, ^3J(H,H) = 5.5 Hz, Os-Ar*H*), 5.75 (d, 1H, ^3J(H,H) = 5.5 Hz, Os-Ar*H*), 5.55 (d, 1H, ^3J(H,H) = 5.0 Hz, Os-Ar*H*), 5.43 (d, 1H, ^3J(H,H) = 5.0 Hz, Os-Ar*H*), 4.65 (s, 1H, NC*H*Ph), 3.88 (d, 1H, ^3J(H,H) = 3.5 Hz, NHC*H*Ph), 2.45–2.34 (m, 1H, Os-ArHC*H*(CH_3)$_2$), 2.18 (s, 3H, Os-ArHCH(CH_3)$_2$), 2.12 (s, 3H, Os-ArHCH(CH_3)$_2$), 1.24 (d, 3H, ^3J(H,H) = 6.5 Hz, Os-ArHCH_3), 1.13 (d, 3H, ^3J(H,H) = 6.5 Hz, SO_2ArHCH_3); ^{13}C NMR (125 MHz, DMSO-d_6, 298 K): δ 146.9, 144.7, 137.5, 131.1, 127.7, 127.4, 126.9, 126.4, 126.0, 123.5, 90.3, 82.0, 79.4, 76.3, 73.4, 71.0, 70.5, 67.0, 32.0, 23.3, 22.9, 20.8, 20.1; UV/Vis λ_{max}, 278, 405, 472 nm; HRMS (ESI): *m*/*z* calcd for $C_{31}H_{35}N_2O_2OsS$ [M + H]$^+$, 691.2034; found, 691.2028. Elemental analysis Calcd (%) for $C_{31}H_{34}N_2O_2OsS$: C, 56.64 (54.60); H, 5.36 (5.30); N, 4.02 (3.98).

*[Os(p-cym)(p–CF_3–BsDPEN)] (**3**).* Synthesized as per the general procedure using [Os(η^6-*p*-cymene)Cl$_2$]$_2$ (58.7 mg, 0.074 mmol, 1 mol equiv) and *N*-((1*R*,2*R*)-2-amino-1,2-diphenylethyl)-3-methylbenzenesulfonamide (***RR*-L2**) (59.0 mg, 0.14 mmol, 2 mol equiv). A rapid color change from a yellow to deep red solution was observed upon addition of KOH (56.1 mg, 1 mmol, 15 mol equiv) addition. The solid was recrystallized from DCM/hexane to yield a dark brown, amorphous solid (44 mg, 0.061 mmol, 93.7%). ^{1}H NMR (500 MHz, DMSO-d_6, 298 K, TMS): δ 8.30 (s, 1H, N*H*), 7.61–7.42 (m, 5H, ArH), 7.24–7.10 (m, 9H, ArH), 6.04 (d, ^3J(H,H) = 5.2 Hz, 1H, F_3CArH), 5.92 (d, ^3J(H,H) = 4.8 Hz, 1H, F_3CArH), 5.84 (d, ^3J(H,H) = 4.8 Hz, 1H, F_3CArH), 5.76 (d, ^3J(H,H) = 5.2 Hz, 1H F_3CArH), 4.26 (s, 1H, NC*H*Ph), 3.90 (d, ^3J(H,H) = 4.0 Hz, 1H, NHC*H*Ph), 2.36–1.99 (m, 4H, ArCH_3 and ArC*H*(CH_3)$_2$), 1.33 (d, 3H, ArCH(CH_3)$_2$), 1.23 (d, ^3J(H,H) = 7.6 Hz, 3H, ArCH(CH_3)$_2$); ^{13}C NMR (125 MHz, DMSO-d_6, 298 K): δ 130.8, 128.7, 128.3, 127.8, 127.4, 127.0, 126.3, 82.6, 74.9, 73.0, 72.2, 68.2, 64.7, 57.5, 22.7, 20.8, 186; UV/Vis λ_{max}, 323, 403, 479 nm; HRMS (ESI): *m*/*z* calcd for $C_{31}H_{31}F_3N_2O_2SOs$ [M + H]$^+$, 745.1674; found, 745.1746. Elemental analysis Calcd (%) for $C_{31}H_{31}F_3N_2O_2OsS$: C, 50.09 (50.12); H, 4.19 (4.21); N, 3.71 (3.77).

*[Os(p-cym)(m–CF_3–BsDPEN)] (**4**).* Synthesized as per the general procedure using [Os(η^6-*p*-cymene)Cl$_2$]$_2$ (54.2 mg, 0.069 mmol, 1 mol equiv) and *N*-((1*R*,2*R*)-2-amino-1,2-diphenylethyl)-4-(trifluoromethyl)benzenesulfonamide (***RR*-L3**) (56.3 mg, 0.14 mmol, 2 mol equiv). A rapid color change from a yellow to a red solution was observed upon addition of KOH (56.1 mg, 1 mmol, 15 mol equiv). The solid was recrystallized from DCM/hexane to yield a dark red amorphous solid (40 mg, 0.062 mmol, 84.4%). ^{1}H NMR

https://doi.org/10.1021/acs.organomet.1c00358
Organometallics XXXX, XXX, XXX–XXX

(500 MHz, DMSO-d_6, 298 K, TMS): δ 8.35 (s, 1H, NH), 7.80−7.70 (m, 1H, ArH), 7.64−7.54 (m, 2H, ArH), 7.52−7.40 (m, 2H, ArH), 7.31−7.09 (m, 9H, ArH), 6.00 (d, ^3J(H,H) = 5.0 Hz, 1H, Os-ArH), 5.88 (d, ^3J(H,H) = 5.0 Hz, 1H, Os-ArH), 5.79 (d, ^3J(H,H) = 5.5 Hz, 1H, Os-ArH), 5.70 (d, ^3J(H,H) = 5 Hz, 1H, Os-ArH), 4.27 (s, 1H, NC*H*Ph), 3.88 (s, 1H, NHC*H*Ph), 2.55 (s, 3H, Os-ArCH_3), 2.33−2.09 (m, 1H, Os-ArCH(CH_3)$_2$), 1.26 (m, 6H, Os-ArCH(CH_3)$_2$); ^{13}C NMR (125 MHz, DMSO-d_6, 298 K): δ 146.0, 145.1, 128.8, 127.7, 126.9, 126.2, 126.0, 82.4, 79.9, 73.0, 71.0, 70.4, 67.0, 32.1, 24.0, 23.0; UV/Vis λ_{max}, 269, 410, 485 nm; HRMS (ESI): m/z calcd for $C_{31}H_{32}F_3N_2O_2OsS$ [M + H]$^+$, 745.1674; found, 745.1745. Elemental analysis Calcd (%) for $C_{31}H_{31}F_3N_2O_2OsS$: C, 50.08 (50.12); H, 4.19 (4.21); N, 3.72 (3.77).

*[Os(p-cym)(p-^{t}Bu-BsDPEN)] (**5**).* Synthesized as per the general procedure using [Os(η^6-*p*-cymene)Cl$_2$]$_2$ (51.4 mg, 0.065 mmol, 1 mol equiv) and *N*-(1*R*,2*R*)-2-amino-(1,2-diphenylethyl)-4-(*tert*-butyl)-benzenesulfonamide (***RR*-L4**) (53.04 mg, 0.130 mmol, 2 mol equiv). A rapid color change from a yellow to a dark orange solution was observed upon addition of KOH (56 mg, 1 mmol, 15 mol equiv). The solid was recrystallized from DCM/hexane to yield a dark orange amorphous solid (49 mg, 0.071 mmol, 98.2%). ^{1}H NMR (500 MHz, DMSO-d_6, 298 K, TMS): δ 8.12 (s, 1H, N*H*), 7.49 (d, ^3J(H,H) = 8.0 Hz, 2H, C*H*CSO$_2$), 7.28−7.22 (m, 8H, ArH), 7.20−7.16 (m, 2H, ArH), 7.12 (d, ^3J(H,H) = 8.0 Hz, 2H, C*H*CHCSO$_2$), 5.90 (d, ^3J(H,H) = 5.5 Hz, 1H, Os-ArH), 5.77 (d, ^3J(H,H) = 6.0 Hz, 1H, Os-ArH), 5.59 (d, ^3J(H,H) = 5.5 Hz, 1H, Os-ArH), 5.41 (d, ^3J(H,H) = 5.5 Hz, 1H, Os-ArH), 4.32 (s, 1H, NC*H*Ar), 3.88 (d, ^3J(H,H) = 4.5 Hz, 1H, NHC*H*Ar), 2.20 (s, 3H, Os-ArCH_3), 2.08 (s, 1H, Os-ArCH(CH$_3$)$_2$), 1.27 (s, 9H, O$_2$SArC(CH_3)$_3$), 1.23 (d, ^3J(H,H) = 7.0 Hz, 3H, Os-ArCH(CH_3)$_2$), 1.10 (d, ^3J(H,H) = 7.0 Hz, 3H, Os-ArCH(CH_3)$_2$); ^{13}C NMR (125 MHz, DMSO-d_6, 298 K): δ 153.1, 146.9, 144.9, 141.9, 127.6, 127.4, 126.9, 126.8, 126.6, 126.2, 126.0, 124.5, 90.2, 82.1, 79.4, 73.6, 31.9, 30.9, 23.2, 20.1; UV/Vis λ_{max}, 262, 406, 474 nm; HRMS (ESI): m/z calcd for $C_{34}H_{41}N_2O_2OsS$ [M + H]$^+$, 733.2426; Found, 733.2490. Elemental analysis Calcd (%) for $C_{34}H_{40}N_2O_2OsS$: C, 55.85 (55.87); H, 5.51 (5.52); N, 3.87 (3.83).

General Synthesis of Osmium Biphenyl Complex. Osmium biphenyl dimer ([Os(η^6-biphenyl)Cl$_2$]$_2$ 1 mol equiv) and benzenesulfonamide ligand (2.15 mol equiv) were stirred in DCM (3 mL) in a microwave vial and then placed in a CEM Discovery-SP microwave reactor for 10 min (393 K, 150 W, 250 psi). To remove any unreacted osmium dimer, the brown solution was filtered and then combined with freshly ground KOH (56.1 mg, 1 mmol, 12 mol equiv). Vigorous stirring was continued for 30 min until a color change from yellow to red-orange was observed. Distilled water (10 mL) was added while stirring for a further 15 min. The aqueous layer was extracted with DCM (3 × 5 mL) and concentrated *in vacuo* to yield a solid, which was recrystallized with DCM/hexane.

*[Os(bip)(m−CH$_3$−BsDPEN)] (**10**).* Synthesized as per the general procedure using [Os(η^6-biphenyl)Cl$_2$]$_2$ (50.4 mg, 0.061 mmol, 1 mol equiv) and *N*-(1*R*,2*R*)-2-amino-(1,2-diphenylethyl)-3-methylbenzenesulfonamide (***RR*-L1**) (44.9 mg, 0.12 mmol, 2 mol equiv). A color change from yellow to dark red solution was observed upon addition of KOH (56.1 mg, 1 mmol, 12 mol equiv) addition. The solid was recrystallized from DCM/hexane to yield a dark orange amorphous solid (35.9 mg, 0.051 mmol, 82.9%). ^{1}H NMR (500 MHz, DMSO-d_6, 298 K, TMS): δ 8.52 (d, ^3J(H,H) = 5.5 Hz, 1H, N*H*CHPh), 7.67−7.64 (m, 2H, SO$_2$Ar*H*), 7.47−7.37 (m, 5H, Os-Ar*H*), 7.21−7.02 (m, 11H, ArH), 6.91 (s, 1H, ArH), 6.43−6.42 (m, 1H, Os-ArH), 6.23−6.20 (m, 1H, Os-ArH), 6.19−6.13 (m, 2H, Os-ArH), 6.07−6.05 (m, 1H, Os-ArH), 4.24 (s, 1H, NC*H*Ph), 3.76 (d, ^3J(H,H) = 4.5 Hz, 1H, NHC*H*Ph), 2.08 (s, 3H, SO$_2$ArHCH_3); ^{13}C NMR (125 MHz, DMSO-d_6, 298 K): δ 146.5, 144.1, 137.9, 137.4, 131.2, 128.7, 128.4, 128.3, 127.7, 127.4, 127.0, 126.5, 126.4, 126.4, 126.0, 123.4, 82.6, 81.5, 75.9, 73.2, 71.4, 70.4, 68.2, 67.4, 20.8; UV/Vis λ_{max}, 269, 415, 490 nm; HRMS (ESI): m/z calcd for $C_{33}H_{31}N_2O_2OsS$ [M + H]$^+$, 711.1721; found, 711.1714. Elemental analysis Calcd (%) for $C_{33}H_{30}N_2O_2OsS$: C, 55.96 (55.91); H, 4.31 (4.27); N, 3.98 (3.95).

*[Os(bip)(p−CF$_3$−BsDPEN)] (**11**).* Synthesized as per the general procedure using [Os(η^6-biphenyl)Cl$_2$]$_2$ (67 mg, 0.081 mmol, 1 mol equiv) and (1*S*,2*S*)-2-amino-(1,2-diphenylethyl)-4-(trifluoromethyl)-benzenesulfonamide (***SS*-L2**) (63 mg, 0.15 mmol, 2 mol equiv). A color change from yellow to a red solution was observed upon the addition of KOH (56.1 mg, 1 mmol, 12 mol equiv). The solid was recrystallized from DCM/hexane to yield a red amorphous solid (50 mg, 0.066 mmol, 81.3%). ^{1}H NMR (500 MHz, DMSO-d_6, 298 K, TMS): δ 8.58 (s, 1H, N*H*), 7.77−7.76 (m, 2H, F$_3$CCC*H*CH), 7.51−7.45 (m, 4H, ArH), 7.38−7.35 (m, 4H, ArH), 7.32−7.31 (m, 2H, F$_3$CCCHC*H*), 7.12−6.91 (m, 7H, ArH), 6.60 (d, ^3J(H,H) = 6.5 Hz, 1H, Os-ArH), 6.48 (d, ^3J(H,H) = 5.0 Hz, 1H, Os-ArH), 6.42 (t, ^3J(H,H) = 5.5 Hz, 1H, Os-ArH), 6.25 (t, ^3J(H,H) = 6.5 Hz, 1H, Os-ArH), 6.21 (t, ^3J(H,H) = 6.5 Hz, 1H, Os-ArH), 4.08 (d, ^3J(H,H) = 1 Hz, 1H, NC*H*Ph), 3.72 (d, ^3J(H,H) = 4.5 Hz, 1H, NHC*H*Ph); ^{13}C NMR (100 MHz, DMSO-d_6, 298 K, TMS): δ 152.1, 145.7, 145.0, 143.8, 137.8, 134.3, 128.7, 128.3, 127.5, 126.7, 126.4, 126.3, 126.2, 126.0, 124.8, 81.6, 56.0, 47.8, 18.6; UV/Vis λ_{max}, 259, 412, 485 nm. HRMS (ESI): m/z calcd for $C_{33}H_{28}F_3N_2O_2OsS$ [M + H]$^+$, 765.1361; found, 765.1336. Elemental analysis Calcd (%) for $C_{33}H_{27}F_3N_2O_2OsS$: C, 52.00 (51.96); H, 3.59 (3.57); N, 3.69 (3.67).

*[Os(bip)(m−CF$_3$−BsDPEN)] (**12**).* Synthesized as per the general procedure using [Os(η^6-biphenyl)Cl$_2$]$_2$ (67.4 mg, 0.081 mmol, 1 mol equiv) and *N*-(1*S*,2*S*)-2-amino-(1,2-diphenylethyl)-3-methylbenzenesulfonamide (***SS*-L3**) (64.06 mg, 0.15 mmol, 2 mol equiv). A color change from yellow to a deep red solution was observed upon addition of KOH (56.1 mg, 1 mmol, 12 mol equiv). The solid was recrystallized from DCM/hexane to yield a dark red amorphous solid (45.6 mg, 0.060 mmol, 74.8%). ^{1}H NMR (500 MHz, DMSO-d_6, 298 K, TMS): δ 8.63 (s, 1H, N*H*), 7.84−7.59 (m, 3H, ArH), 7.57−7.21 (m, 8H, ArH), 7.16−6.83 (m, 8H, ArH), 6.53 (s, 1H, Os-ArH), 6.45−6.28 (m, 2H, Os-ArH), 6.25−6.12 (m, 1H, Os-ArH), 5.74 (s, 1H, Os-ArH), 4.10 (s, 1H NC*H*Ph), 4.71 (s, 1H NHC*H*Ph); ^{13}C NMR (125 MHz, DMSO-d_6, 298 K): δ 145.5, 144.6, 144.7, 137.7, 129.5, 128.9, 128.7, 128.3, 127.6, 127.4, 126.9, 126.7, 126.1, 82.9, 81.8, 75.0, 72.7, 72.2, 71.1, 68.6, 67.8, 54.9; UV/Vis λ_{max}, 289, 365, 512 nm; HRMS (ESI): m/z calcd for $C_{33}H_{28}F_3N_2O_2SOs$ [M + H]$^+$, 765.1438; found, 765.1437. Elemental analysis Calcd (%) for $C_{33}H_{27}F_3N_2O_2SOs$: C, 52.01 (51.96); H, 3.60 (3.57); N, 3.71 (3.67).

*[Os(bip)(p-^{t}Bu-BsDPEN)] (**13**).* Synthesized as per the general procedure previously stated using [Os(η^6-biphenyl)Cl$_2$]$_2$ (59.8 mg, 0.072 mmol, 1 mol equiv) and *N*-(1*R*,2*R*)-2-amino-(1,2-diphenylethyl)-4-fluorobenzenesulfonamide (***RR*-L4**) (61.23 mg, 0.15 mmol, 2 mol equiv). A color change from yellow to a deep red solution was observed upon the addition of KOH (56 mg, 1 mmol, 12 mol equiv). The solid was recrystallized from DCM/hexane to yield a red amorphous solid (48 mg, 0.06 mmol, 78.2%). ^{1}H NMR (500 MHz, DMSO-d_6, 298 K, TMS): δ 8.48 (d, 1H, ^3J(H,H) = 5.0 Hz, N*H*), 7.71−7.66 (m, 2H, SO$_2$Ar*H*), 7.50−7.43 (m, 3H, ArH), 7.38−7.33 (m, 2H, SO$_2$ArH), 7.16−7.06 (m, 8H, ArH), 7.03−6.95 (m, 4H, ArH), 6.47 (d, 1H, ^3J(H,H) = 5.5 Hz, Os-ArH), 6.33−6.28 (m, 1H, Os-ArH), 6.18−6.15 (m, 2H, Os-ArH), 6.14 (t, 1H, ^3J(H,H) = 5.5 Hz, Os-ArH), 4.12 (s, 1H, NC*H*Ph), 4.72 (d, 1H, ^3J(H,H) = 4.0 Hz, NHC*H*Ph), 1.26 (s, 9H, SO$_2$ArHC(CH_3)$_3$); ^{13}C NMR (125 MHz, DMSO-d_6, 298 K): δ 152.9, 146.4, 144.0, 141.0, 137.9, 128.9, 128.7, 128.4, 127.5, 127.4, 126.9, 126.7, 126.4, 125.9, 124.5, 82.9, 81.6, 76.0, 74.0, 71.8, 70.0, 68.4, 67.6, 30.9; UV/Vis λ_{max}, 278, 412, 487 nm; HRMS (ESI): m/z calcd for $C_{36}H_{37}N_2O_2OsS$ [M + H]$^+$, 753.2191; found, 753.2191. Elemental analysis Calcd (%) for $C_{36}H_{36}N_2O_2OsS$: C, 57.61 (57.58); H, 4.86 (4.83)' N, 3.77 (3.73).

*[Os(bip)(p-F-BsDPEN)] (**14**).* [Os(η^6-biphenyl)Cl$_2$]$_2$ and *N*-(1*R*,2*R*)-2-amino-(1,2-diphenylethyl)-4-fluorobenzenesulfonamide were synthesized as previously described.[21] Complex **14** was synthesized as per the general procedure previously stated using [Os(η^6-biphenyl)Cl$_2$]$_2$ (70 mg, 0.084 mmol, 1 mol equiv) and *N*-(1*R*,2*R*)-2-amino-(1,2-diphenylethyl)-4-fluorobenzenesulfonamide (57 mg, 0.161 mmol, 2 mol equiv).[21] A color change from yellow to deep red was observed upon addition of KOH (57 mg, 1 mmol, 12 mol equiv). The solid was recrystallized from DCM/hexane to yield a dark red amorphous solid (49.1 mg, 0.0491 mmol, 84.9%). ^{1}H NMR

https://doi.org/10.1021/acs.organomet.1c00358
Organometallics XXXX, XXX, XXX−XXX

(500 MHz, DMSO-d_6, 298 K, TMS): δ 8.52 (s, 1H, NH), 7.77−7.72 (m, 2H, FCCH), 7.70−7.34 (m, 7H, ArH), 7.24−7.19 (t, ^3J(H,H) = 5.5 Hz, 2H, FCCHCH), 7.17−7.07 (m, 3H, ArH), 7.06−6.98 (m, 2H, ArH), 6.98−6.92 (m, 2H, ArH), 6.91−6.77 (m, 3H, ArH), 6.55 (d, ^3J(H,H) = 6.0 Hz, 1H, Os-ArH), 6.38 (d, ^3J(H,H) = 5.5 Hz, 1H, Os-ArH), 6.32 (t, ^3J(H,H) = 5.5 Hz, 1H, Os-ArH), 6.18 (t, ^3J(H,H) = 6.0 Hz, 1H, Os-ArH), 6.13 (d, ^3J(H,H) = 5.5 Hz, 1H, Os-ArH), 4.11 (s, 1H, NCHPh), 4.73 (d, ^3J(H,H) = 4.0 Hz, 1H, NHCHPh); ^{13}C NMR (125 MHz, DMSO-d_6, 298 K): δ 146.0, 144.0, 140.1, 137.8, 128.0, 128.7, 128.5, 128.4, 128.3, 127.6, 127.4, 126.7, 126.6, 126.4, 126.0, 114.6, 74.5, 74.0; UV/Vis λ_{max}, 260, 417, 486 nm; HRMS (ESI): m/z calcd for $C_{32}H_{28}FN_2O_2OsS$ $[M + H]^+$, 715.1394; found, 715.1464. Elemental analysis Calcd (%) for $C_{32}H_{27}FN_2O_2OsS$: C, 54.87 (54.92); H, 4.86 (4.82); N, 4.94 (4.93).

*[Os(bip)(p-Br-BsDPEN)] (**15**).* $[Os(\eta^6\text{-biphenyl})Cl_2]_2$ and (1*R*,2*R*)-2-amino-(1,2-diphenylethyl)-4-bromobenzenesulfonamide were synthesized as previously described.[21,23] Complex **15** was synthesized as per the general procedure previously stated using $[Os(\eta^6\text{-biphenyl})Cl_2]_2$ (68.0 mg, 0.082 mmol, 1 mol equiv) and *N*-(1*R*,2*R*)-2-amino-(1,2-diphenylethyl)-4-bromobenzenesulfonamide (66 mg, 0.15 mmol, 2 mol equiv). A color change from yellow to deep red solution was observed upon the addition of KOH (56.1 mg, 1 mmol, 12 mol equiv). The solid was recrystallized from DCM/hexane to yield a dark red amorphous solid (40 mg, 0.0426 mmol, 64.9%). ^{1}H NMR (500 MHz, DMSO-d_6, 298 K, TMS): δ 8.53 (s, 1H, NH), 7.77−7.61 (m, 2H, F_3CCCH), 7.52−7.29 (m, 5H, ArH), 7.24−6.76 (m, 12H, ArH), 6.59−6.47 (m, 1H, Os-ArH), 6.42−6.26 (m, 2H, Os-ArH), 6.22−6.00 (m, 2H, Os-ArH), 4.08 (s, 1H, NCHPh), 4.72 (d, 1H, ^3J(H,H) = 5.0 Hz, NHCHPh); ^{13}C NMR (125 MHz, DMSO-d_6, 298 K): δ 147.6, 145.7, 144.6, 144.3, 138.4, 131.4, 129.8, 128.8, 127.6, 127.4, 126.9, 126.7, 126.3, 126.1, 124.0, 82.2, 74.9, 69.3, 61.0, 57.9, 52.7, 48.8, 24.8; UV/Vis, λ_{max}, 256, 318, 549.6 nm; HRMS (ESI): m/z calcd for $C_{32}H_{28}BrN_2O_2OsS$ $[M + H]^+$, 775.0592; found, 775.0644. Elemental analysis Calcd (%) for $C_{32}H_{27}BrN_2O_2OsS$: C, 49.70 (49.67); H, 4.56 (4.52); N, 4.67 (4.62).

*[Os(bip)(p-I-BsDPEN)] (**16**).* $[Os(\eta^6\text{-biphenyl})Cl_2]_2$ and (1*S*,2*S*)-2-amino-1,2-diphenylethyl)-4-iodobenzenesulfonamide were synthesized as previously described.[21,23] Complex **16** was synthesized as per the general procedure previously stated using $[Os(\eta^6\text{-biphenyl})Cl_2]_2$ (67.9 mg, 0.082 mmol, 1 mol equiv) and *N*-(1*S*,2*S*)-2-amino-(1,2-diphenylethyl)-4-iodobenzenesulfonamide (98 mg, 0.16 mmol, 2 mol equiv). A color change from yellow to deep red solution was observed upon the addition of KOH (56.1 mg, 1 mmol, 12 mol equiv). The solid was recrystallized from DCM/hexane to yield a red amorphous solid (57 mg, 0.069 mmol, 85.2%).^{1}H NMR (500 MHz, DMSO-d_6, 298 K, TMS): δ 8.54 (s, 1H, NH), 7.72−7.66 (m, 2H, IC(CH)$_2$(CH)$_2$), 7.50−7.42 (m, 3H, ArH), 7.40−7.33 (m, 4H, ArH), 7.19−7.08 (m, 4H, ArH), 7.04−6.97 (m, 2H, IC(CH)$_2$(CH)$_2$), 6.96−6.89 (m, 4H, ArH), 6.53 (d, ^3J(H,H) = 7.0 Hz, 1H, Os-ArH), 6.34 (t, ^3J(H,H) = 7.0 Hz, 2H, Os-ArH), 6.19 (t, ^3J(H,H) = 7.0 Hz, 1H, Os-ArH), 6.14 (t, ^3J(H,H) = 7.0 Hz, 1H, Os-ArH), 4.08 (s, 1H, NCHPh), 4.72 (d, ^3J(H,H) = 5.5 Hz, 1H, NHCHPh); ^{13}C NMR (125 MHz, DMSO-d_6, 298 K): δ 146.1, 144.8, 144.2, 137.7, 136.7, 128.9, 128.7, 128.4, 128.3, 127.6, 127.4, 127.0, 126.7, 126.4, 126.3, 126.0, 82.7, 74.0, 72.1, 68.5; UV/Vis λ_{max}, 329, 411, 489 nm; HRMS (ESI): m/z calcd for $C_{32}H_{28}IN_2O_2OsS$ $[M + H]^+$, 824.0531; found, 824.0525. Elemental analysis Calcd (%) for $C_{32}H_{27}IN_2O_2OsS$: C, 46.89 (46.83); H, 4.36 (4.32); N, 4.39 (4.41).

Chiral GC. *General Chiral GC Method.* Under a nitrogen atmosphere, the osmium complex (1 mol equiv) was dissolved in 5:2 formic acid/triethylamine (500 μL), followed by addition of acetophenone-derived substrate (200 mol equiv) and stirred for 24 h (310 K). One drop of reaction mixture was combined with saturated sodium hydrogen carbonate (1 mL) and ethyl acetate (1 mL) and filtered through a column of silica. Samples were then analyzed by chiral GC to determine *ee* and conversions (%). Chiral GC measurements were carried out by Jonathan Barrios-Rivera and Sam Forshaw (University of Warwick) on a Hewlett-Packard 5890 instrument linked to PC running DataApex Clarity software. Measurements were obtained using a CROMPAC CYCLODEX-TRIN-β-236M-19, 50 m × 0.25 mm × 0.25 μm, carrier gas = H_2, T = 383 K, pressure = 15 psi, FID temperature = 523 K, injection temperature = 493 K. Data were analyzed on Windows Clarity Chromatography Suite.

Reduction of Acetophenone. Reactions were performed as per the general chiral GC procedure using complexes **1**−**16** (5 μmol, 1 mol equiv), 5:2 formic acid/triethylamine (500 μL), and acetophenone substrate (0.117 mL, 1 mmol, 200 mol equiv), using optically pure (*R*) and (*S*) 1-phenylethanol samples as standards.

Reduction of 2-Chloroacetophenone. Reactions were performed as per general chiral GC procedure previously stated using complexes **5** and **13** (0.76 μmol, 1 mol equiv), 5:2 formic acid/triethylamine (500 μL), and 2-chloroacetophenone substrate (23.5 mg, 152 μmol, 200 mol equiv), using optically pure (*R*) and (*S*) 2-chloro-1-phenylethanol alcohol samples as standards.[46]

Reduction of 4-Methoxyacetophenone. Reactions were performed as per general chiral GC procedure previously stated using complexes **5** and **13** (0.76 μmol, 1 mol equiv), 5:2 formic acid/triethylamine (500 μL), and 4-methoxyacetophenone (20.4 mg, 152 μmol, 200 mol equiv), using optically pure (*R*) and (*S*) 1-(4-methoxyphenyl)ethanol samples as standards.[46]

^{1}H NMR Kinetic Studies for the Reduction of Acetophenone-Derived Substrates. *General ^{1}H NMR Kinetic Studies Method.* Under a nitrogen atmosphere, osmium complexes (1 mol equiv) were dissolved in deuterated benzene (100 μL) and vigorously stirred with 5:2 formic acid/triethylamine (500 μL) for 30 min. The substrate (200 mol equiv) was combined with the reaction mixture which was transferred to an NMR tube (5 mm diameter) with a pieced lid. The reaction was monitored at 310 K in a Bruker AVANCE III HD 400 MHz spectrometer and done in triplicate for statistical coherence. In each triplicate, two reactions were monitored for 2 h, whereby the final reaction was observed for 12 h to establish reaction completion. The average turnover number (TON) used was calculated, and hence, the TOF (h^{-1}) was derived. Experiments were conducted at physiological temperature (310 K) for biological relevance. Statistics were compared using Welch's *t*-test at the 95% confidence limit.

Reduction of Acetophenone. Reactions were as per general ^{1}H NMR kinetic study procedure previously stated using complexes **1**−**16** (5 μmol, 1 mol equiv), d_6-benzene (100 μL), 5:2 formic acid/triethylamine (500 μL), and acetophenone substrate (0.117 mL, 1 mmol, 200 mol equiv).

Reduction of 2-Chloroacetophenone. Reactions were performed as per the general ^{1}H NMR kinetic study procedure previously stated using complex **1**, **5**, **13**, and **16** (0.76 μmol, 1 mol equiv), d_6-benzene (100 μL), 5:2 formic acid/triethylamine (500 μL), and 2-chloroacetophenone substrate (23.5 mg, 152 μmol, 200 mol equiv).

4-Methoxyacetophenone ^{1}H NMR Kinetic Studies. Reactions were performed as per the general ^{1}H NMR kinetic study procedure previously stated using **5** and **13** (0.76 μmol, 1 mol equiv), d_6-benzene (100 μL), 5:2 formic acid/triethylamine (500 μL), and 4-methoxyacetophenone substrate (20.4 mg, 152 μmol, 200 mol equiv).

Catalytic Reduction of Quinones. *General ^{1}H NMR Kinetic Studies.* Under a nitrogen atmosphere, osmium complexes (1 mol equiv) were vigorously stirred in 5:2 formic acid/triethylamine (300 μL) for 30 min. Simultaneously, the quinone substrate (200 mol equiv) was dissolved and vigorously stirred in deuterated benzene (200 μL) and 5:2 formic acid/triethylamine (200 μL) for 30 min. The two reaction mixtures were combined and transferred into an NMR tube (5 mm diameter) with a pieced lid. The reaction was monitored by ^{1}H NMR at 310 K; TOF calculated as stated previously in acetophenone kinetic studies.

Reduction of Duroquinone. Reactions were performed as per the general ^{1}H NMR kinetic study procedure using complexes **1**, **5**, **13**, and **16** (0.76 μmol, 1 mol equiv), d_6-benzene (200 μL), 5:2 formic acid/triethylamine (500 μL), and duroquinone (25 mg, 0.152 mmol, 200 mol equiv).

Reduction of Menadione. Reactions were performed as per general ^{1}H NMR kinetic study procedure using complexes **5** and **13** (0.76 μmol, 1 mol equiv), d_6-benzene (200 μL), 5:2 formic acid/

https://doi.org/10.1021/acs.organomet.1c00358
Organometallics XXXX, XXX, XXX−XXX

triethylamine (500 μL), and menadione (26.2 mg, 0.152 mmol, 200 mol equiv).

Determination of Duroquinone Reduction Product. Reactions were performed as per the general product determination procedure using complex **5** (1.52 μmol, 1 mol equiv), 5:2 formic acid/triethylamine (500 μL) and duroquinone (25.0 mg, 0.152 mmol, 100 mol equiv), and yellow crystals. This yielded a brown crystalline solid (21.6 mg, 0.130 mmol, 85.5%). ^{1}H NMR (500 MHz, DMSO-d_6, 298 K, TMS): δ 7.33 (s, 2H, O*H*), 2.06 (s, 12H, CH_3); ^{13}C NMR (125 MHz, DMSO-d_6, 298 K): δ 146.1, 121.8, 13.4. Further analyzed by ^{1}H−^{1}H COSY (resolution insufficient for publication), ^{1}H−^{13}C HSQC and ^{1}H−^{13}C HMBC NMR spectroscopy. LRMS (ESI): m/z calcd for $C_{15}H_{17}O_2N_2$ [M + 2Na−H]$^+$, 211.1; found, 211.3.

Determination of Menadione Reduction Product. Reactions were performed as per the general product determination procedure using complex **13** (1.52 μmol, 1 mol equiv), 5:2 formic acid/triethylamine (500 μL) and menadione (26.2 mg, 0.152 mmol, 100 mol equiv, yellow powder). This yielded a purple crystalline solid (21.9 mg, 0.126 mmol, 82.7%). ^{1}H NMR (500 MHz, DMSO-d_6, 298 K, TMS): δ 9.39 (s, 1H, *H*OCCH), 8.29 (s, 1H, *H*OCC(CH$_3$)), 8.10 (d, ^3J(H,H) = 8.4 Hz, 1H, Ph*H*), 8.04 (d, ^3J(H,H) = 8.4 Hz, 1H, Ph*H*), 7.43 (t, ^3J(H,H) = 7.2 Hz, 1H, Ph*H*), 7.36 (t, ^3J(H,H) = 7.2 Hz, 1H, Ph*H*), 6.66 (s, 1H, HOCC*H*C(CH$_3$)), 2.31 (s, 3H, HOCC(CH_3)); ^{13}C NMR (125 MHz, DMSO-d_6, 298 K): δ 146.2, 142.2, 127.0, 125.4, 124.3, 124.0, 122.3, 122.1, 119.1, 111.8, 17.0. Analyzed by ^{1}H−^{1}H COSY, ^{1}H−^{13}C HSQC and ^{1}H−^{13}C HMBC NMR spectroscopy; LRMS (ESI): m/z calcd for $C_{15}H_{17}O_2N_2$ [M + 2ACN + H]$^+$, 257.1; found, 257.2.

CONCLUSIONS

Organo-osmium(II) complexes [Os^{II}(η^6-arene)(R-PhDPEN)] can catalyze reduction of prochiral ketones to optically pure alcohols in the presence of a hydride source. We are particularly interested in the use of synthetic catalysts for transfer hydrogenation reactions in cells, for which these Os(II) complexes have potential advantages over their better-known Ru(II) analogues, being highly active and stable as active 16-electron catalysts. To improve their catalytic performance, we have introduced electron-donor and electron-acceptor substituents (R) into the *para* (R_1) or *meta* (R_2) positions of the chiral R-phenyl-sulfonyl-diphenylethyl-enediamine (Ph-DPEN) ligands and for the first time explored the reduction of quinones, potential biological substrates which play major roles in cellular electron transfer chains. These complexes exhibited remarkably high turnover frequencies toward reduction of acetophenone-derived substrates in the presence of formic acid, with high enantioselectivity (>92%) and conversions (>93%). Interestingly, the catalytic activity of such complexes was improved with the *tert*-butyl substituent in the *para*-position, achieving TOFs more than 40% higher than that of the parent *methyl*-substituted complexes, while maintaining high enantioselectivity (>98%) and conversions (>98%). Consequently, these *tert*-butyl-containing catalysts were screened for the reduction of quinones.

Biological quinones can provide protection to cells by modification of redox homeostasis in response to stress (e.g., chemotherapeutics). The two-electron reduction of quinones is a major detoxification mechanism for quinones; thus, research into quinones as substrates for in-cell catalysis is of significant interest. Here, we investigated the reduction of quinones by this family of organo-osmium(II) catalysts in the presence of formic acid. The kinetic reduction of duroquinone and menadione to their di-alcohol derivatives (durohydroquinone and menadiol, respectively) exhibited promising conversions (>87%) and TOF (>36 h^{-1}). Interestingly, the TOFs were significantly higher for the less sterically hindered menadione over duroquinone, with a TOF of 145 ± 3 h^{-1} for **13**. In order the further probe this, we used DFT to investigate the catalytic reduction of duroquinone in the presence of such complexes, The DFT calculations revealed interesting features in the mechanism, involving formic acid deprotonation assisted by the catalyst amine groups, phenyl-duroquinone stacking, hydride transfer to Os^{II}, possible CO_2 coordination and tilting of the η^6-arene ring, followed by hydride transfer to the quinone. Notably, we were unable to optimize any structure with the HCO_2^- bound to the osmium, yet, for the ruthenium analogue, the Ru−HCO_2^- coordination was found with a Ru−H distance of 1.72 Å.

Overall, this study provides the first evidence for the reduction of quinones by this family of osmium catalysts, demonstrating their remarkable substrate versatility for transfer hydrogenation reactions. Optimization of such catalysts under biologically relevant conditions may give rise to novel catalytic mechanisms for destroying cells and treating cancer.

ASSOCIATED CONTENT

Supporting Information

The Supporting Information is available free of charge at https://pubs.acs.org/doi/10.1021/acs.organomet.1c00358.

NMR for the catalytic reduction of acetophenone, 2-chloroacetophenone, 4-methoxyactophenone, duroquinone, and menadione using **5** (PDF)
DFT file for intermediate **1** (PDB)
DFT file for intermediate **2** (PDB)
DFT file for intermediate **3a** (PDB)
DFT file for intermediates **3b** (PDB)
DFT file for the Ru analogue of intermediate **3a** (PDB)

AUTHOR INFORMATION

Corresponding Author

Peter J. Sadler − *Department of Chemistry, University of Warwick, Coventry CV4 7AL, U.K.*; orcid.org/0000-0001-9160-1941; Email: p.j.sadler@warwick.ac.uk

Authors

Elizabeth M. Bolitho − *Department of Chemistry, University of Warwick, Coventry CV4 7AL, U.K.*

Nathan G. Worby − *Department of Chemistry, University of Warwick, Coventry CV4 7AL, U.K.*

James P. C. Coverdale − *Department of Chemistry, University of Warwick, Coventry CV4 7AL, U.K.*

Juliusz A. Wolny − *Fachbereich Physik, Technische Universität Kaiserslautern, D-67663 Kaiserslautern, Germany*

Volker Schünemann − *Fachbereich Physik, Technische Universität Kaiserslautern, D-67663 Kaiserslautern, Germany*

Complete contact information is available at: https://pubs.acs.org/10.1021/acs.organomet.1c00358

Notes

The authors declare no competing financial interest.
[§]E.M.B. and N.G.W. shared first author.

ACKNOWLEDGMENTS

We thank Diamond Light Source and Warwick Collaborative Postgraduate Research Scholarship (PhD award for E.M.B.), the Engineering and Physical Sciences Research Council

(EPSRC grant no EP/P030572/1). We thank J. Barrios-Rivera and S. Forshaw (University of Warwick) for assistance with chiral GC−FID measurements, L. Song for mass spectrometry, I. Prokes for NMR spectroscopy, and Heraeus for the gift of osmium trichloride. V.S. and J.A.W. acknowledge support by the research initiative NANOKAT, as well as Allianz für Hochleistungsrechnen Rheinland−Pfalz (AHRP) for providing CPU-time within the project TUK-SPINPLUSVIB.

REFERENCES

(1) Bozan, A.; Songür, R.; Mehmetoğlu, Ü. The production of enantiomerically pure 1-phenylethanol by enzymatic kinetic resolution method using response surface methodology. *Turk. J. Chem.* **2020**, *44*, 1352−1365.
(2) Liu, W.; Gan, J.; Schlenk, D.; Jury, W. A. Enantioselectivity in environmental safety of current chiral insecticides. *Proc. Natl. Acad. Sci. U.S.A.* **2005**, *102*, 701−706.
(3) Knowles, W. S.; Noyori, R. Pioneering Perspectives on Asymmetric Hydrogenation. *Acc. Chem. Res.* **2007**, *40*, 1238−1239.
(4) Noyori, R.; Ohkuma, T. Asymmetric Catalysis by Architectural and Functional Molecular Engineering: Practical Chemo- and Stereoselective Hydrogenation of Ketones. *Angew. Chem., Int. Ed.* **2001**, *40*, 40−73.
(5) Noyori, R.; Ohkuma, T.; Kitamura, M.; Takaya, H.; Sayo, N.; Kumobayashi, H.; Akutagawa, S. Asymmetric hydrogenation of .beta.-keto carboxylic esters. A practical, purely chemical access to .beta.-hydroxy esters in high enantiomeric purity. *J. Am. Chem. Soc.* **1987**, *109*, 5856−5858.
(6) Shende, V. S.; Shingote, S. K.; Deshpande, S. H.; Kuriakose, N.; Vanka, K.; Kelkar, A. A. Asymmetric transfer hydrogenation of imines in water/methanol co-solvent system and mechanistic investigation by DFT study. *RSC Adv.* **2014**, *4*, 46351−46356.
(7) Ohkuma, T. Asymmetric hydrogenation of ketones: tactics to achieve high reactivity, enantioselectivity, and wide scope. *Proc. Jpn. Acad., Ser. B* **2010**, *86*, 202−219.
(8) Sandoval, C. A.; Ohkuma, T.; Muñiz, K.; Noyori, R. Mechanism of asymmetric hydrogenation of ketones catalyzed by BINAP/1,2-diamine-ruthenium(II) complexes. *J. Am. Chem. Soc.* **2003**, *125*, 13490−13503.
(9) Noyori, R.; Hashiguchi, S. Asymmetric Transfer Hydrogenation Catalyzed by Chiral Ruthenium Complexes. *Acc. Chem. Res.* **1997**, *30*, 97−102.
(10) Clapham, S. E.; Hadzovic, A.; Morris, R. H. Mechanisms of the H2-hydrogenation and transfer hydrogenation of polar bonds catalyzed by ruthenium hydride complexes. *Coord. Chem. Rev.* **2004**, *248*, 2201−2237.
(11) Wang, C.; Wu, X.; Xiao, J. Broader, Greener, and More Efficient: Recent Advances in Asymmetric Transfer Hydrogenation. *Chem.−Asian J.* **2008**, *3*, 1750−1770.
(12) Ikariya, T.; Blacker, A. J. Asymmetric Transfer Hydrogenation of Ketones with Bifunctional Transition Metal-Based Molecular Catalysts. *Acc. Chem. Res.* **2007**, *40*, 1300−1308.
(13) Václavík, J.; Šot, P.; Vilhanová, B.; Pecháček, J.; Kuzma, M.; Kačer, P. Practical Aspects and Mechanism of Asymmetric Hydrogenation with Chiral Half-Sandwich Complexes. *Molecules* **2013**, *18*, 6804−6828.
(14) Gladiali, S.; Alberico, E. Asymmetric transfer hydrogenation: chiral ligands and applications. *Chem. Soc. Rev.* **2006**, *35*, 226−236.
(15) Fujii, A.; Hashiguchi, S.; Uematsu, N.; Ikariya, T.; Noyori, R. Ruthenium(II)-Catalyzed Asymmetric Transfer Hydrogenation of Ketones Using a Formic Acid−Triethylamine Mixture. *J. Am. Chem. Soc.* **1996**, *118*, 2521−2522.
(16) Ikariya, T.; Murata, K.; Noyori, R. Bifunctional transition metal-based molecular catalysts for asymmetric syntheses. *Org. Biomol. Chem.* **2006**, *4*, 393−406.
(17) Uematsu, N.; Fujii, A.; Hashiguchi, S.; Ikariya, T.; Noyori, R. Asymmetric Transfer Hydrogenation of Imines. *J. Am. Chem. Soc.* **1996**, *118*, 4916−4917.
(18) Hashiguchi, S.; Fujii, A.; Takehara, J.; Ikariya, T.; Noyori, R. Asymmetric Transfer Hydrogenation of Aromatic Ketones Catalyzed by Chiral Ruthenium(II) Complexes. *J. Am. Chem. Soc.* **1995**, *117*, 7562−7563.
(19) Yamakawa, M.; Yamada, I.; Noyori, R. CH/π Attraction: The Origin of Enantioselectivity in Transfer Hydrogenation of Aromatic Carbonyl Compounds Catalyzed by Chiral η^6-Arene-Ruthenium(II) Complexes. *Angew. Chem., Int. Ed.* **2001**, *40*, 2818−2821.
(20) Coverdale, J. P. C.; Romero-Canelón, I.; Sanchez-Cano, C.; Clarkson, G. J.; Habtemariam, A.; Wills, M.; Sadler, P. J. Asymmetric transfer hydrogenation by synthetic catalysts in cancer cells. *Nat. Chem.* **2018**, *10*, 347−354.
(21) Coverdale, J. P. C.; Sanchez-Cano, C.; Clarkson, G. J.; Soni, R.; Wills, M.; Sadler, P. J. Easy To Synthesize, Robust Organo-osmium Asymmetric Transfer Hydrogenation Catalysts. *Chem.—Eur. J.* **2015**, *21*, 8043−8046.
(22) Coverdale, J. P. C.; Bridgewater, H. E.; Song, J.-I.; Smith, N. A.; Barry, N. P. E.; Bagley, I.; Sadler, P. J.; Romero-Canelón, I. In Vivo Selectivity and Localization of Reactive Oxygen Species (ROS) Induction by Osmium Anticancer Complexes That Circumvent Platinum Resistance. *J. Med. Chem.* **2018**, *61*, 9246−9255.
(23) Bolitho, E. M.; Coverdale, J. P. C.; Bridgewater, H. E.; Clarkson, G. J.; Quinn, P. D.; Sanchez-Cano, C.; Sadler, P. J. Tracking Reactions of Asymmetric Organo-Osmium Transfer Hydrogenation Catalysts in Cancer Cells. *Angew. Chem., Int. Ed.* **2021**, *60*, 6462−6472.
(24) Bolton, J. L.; Dunlap, T. Formation and Biological Targets of Quinones: Cytotoxic versus Cytoprotective Effects. *Chem. Res. Toxicol.* **2017**, *30*, 13−37.
(25) Colucci, M. A.; Couch, G. D.; Moody, C. J. Natural and synthetic quinones and their reduction by the quinone reductase enzyme NQO1: from synthetic organic chemistry to compounds with anticancer potential. *Org. Biomol. Chem.* **2008**, *6*, 637−656.
(26) Tie, J.-K.; Jin, D.-Y.; Straight, D. L.; Stafford, D. W. Functional study of the vitamin K cycle in mammalian cells. *Blood* **2011**, *117*, 2967−2974.
(27) Bona, A. B.; Calcagno, D. Q.; Ribeiro, H. F.; Muniz, J. A. P. C.; Pinto, G. R.; Rocha, C. A. M.; Junior, A. C. C. L.; Assumpção, P. P. d.; Herranz, J. A. R.; Burbano, R. R. Menadione reduces CDC25B expression and promotes tumor shrinkage in gastric cancer. *Ther. Adv. Gastroenterol.* **2020**, *13*, 1756284819895435.
(28) Teixeira, J.; Amorim, R.; Santos, K.; Soares, P.; Datta, S.; Cortopassi, G. A.; Serafim, T. L.; Sardão, V. A.; Garrido, J.; Borges, F.; Oliveira, P. J. Disruption of mitochondrial function as mechanism for anti-cancer activity of a novel mitochondriotropic menadione derivative. *Toxicology* **2018**, *393*, 123−139.
(29) Kang, G.; Lin, S.; Shiwakoti, A.; Ni, B. Imidazolium ion tethered TsDPENs as efficient water-soluble ligands for rhodium catalyzed asymmetric transfer hydrogenation of aromatic ketones. *Catal. Commun.* **2014**, *57*, 111−114.
(30) Tönnemann, J.; Risse, J.; Grote, Z.; Scopelliti, R.; Severin, K. Efficient and Rapid Synthesis of Chlorido-Bridged Half-Sandwich Complexes of Ruthenium, Rhodium, and Iridium by Microwave Heating. *Eur. J. Inorg. Chem.* **2013**, *2013*, 4558−4562.
(31) Dub, P. A.; Gordon, J. C. The mechanism of enantioselective ketone reduction with Noyori and Noyori−Ikariya bifunctional catalysts. *Dalton Trans.* **2016**, *45*, 6756−6781.
(32) Brandt, P.; Roth, P.; Andersson, P. G. Origin of Enantioselectivity in the Ru(arene)(amino alcohol)-Catalyzed Transfer Hydrogenation of Ketones. *J. Org. Chem.* **2004**, *69*, 4885−4890.
(33) Handgraaf, J.-W.; Meijer, E. J. Realistic Modeling of Ruthenium-Catalyzed Transfer Hydrogenation. *J. Am. Chem. Soc.* **2007**, *129*, 3099−3103.
(34) Rawn, J. D.; Ouellette, R. J. *Organic Chemistry: Structure, Mechanism, Synthesis*; Academic Press: London, 2018.
(35) Bolton, J. L.; Trush, M. A.; Penning, T. M.; Dryhurst, G.; Monks, T. J. Role of quinones in toxicology. *Chem. Res. Toxicol.* **2000**, *13*, 135−160.

https://doi.org/10.1021/acs.organomet.1c00358
Organometallics XXXX, XXX, XXX−XXX

(36) Dobrinescu, C.; Iorgulescu, E. E.; Mihailciuc, C.; Macovei, D.; Wuttke, S.; Kemnitz, E.; Parvulescu, V. I.; Coman, S. M. One-Pot Hydroacetylation of Menadione (Vitamin K3) to Menadiol Diacetate (Vitamin K4) by Heterogeneous Catalysis. *Adv. Synth. Catal.* **2012**, *354*, 1301−1306.
(37) Beck, R.; Verrax, J.; Dejeans, N.; Taper, H.; Calderon, P. B. Menadione reduction by pharmacological doses of ascorbate induces an oxidative stress that kills breast cancer cells. *Int. J. Toxicol.* **2009**, *28*, 33−42.
(38) Gui, D. Y.; Sullivan, L. B.; Luengo, A.; Hosios, A. M.; Bush, L. N.; Gitego, N.; Davidson, S. M.; Freinkman, E.; Thomas, C. J.; Vander Heiden, M. G.; Matthew, G. Environment Dictates Dependence on Mitochondrial Complex I for NAD+ and Aspartate Production and Determines Cancer Cell Sensitivity to Metformin. *Cell Metab.* **2016**, *24*, 716−727.
(39) Luengo, A.; Li, Z.; Gui, D. Y.; Sullivan, L. B.; Zagorulya, M.; Do, B. T.; Ferreira, R.; Naamati, A.; Ali, A.; Lewis, C. A.; Thomas, C. J.; Spranger, S.; Matheson, N. J.; Vander Heiden, M. G. Increased demand for NAD(+) relative to ATP drives aerobic glycolysis. *Mol. Cell* **2021**, *81*, 691−707.
(40) Coverdale, J. P. C. *Catalytic Organometallic Anticancer Complexes*; PhD thesis, University of Warwick, 2017.
(41) Orio, M.; Pantazis, D. A.; Neese, F. Density functional theory. *Photosynth. Res.* **2009**, *102*, 443−453.
(42) Becke, A. D. A new mixing of Hartree−Fock and local density-functional theories. *J. Chem. Phys.* **1993**, *98*, 1372−1377.
(43) Stevens, W. J.; Krauss, M.; Basch, H.; Jasien, P. G. Relativistic compact effective potentials and efficient, shared-exponent basis sets for the third-, fourth-, and fifth-row atoms. *Can. J. Chem.* **1992**, *70*, 612−630.
(44) Grimme, S.; Antony, J.; Ehrlich, S.; Krieg, H. A consistent and accurate ab initio parametrization of density functional dispersion correction (DFT-D) for the 94 elements H-Pu. *J. Chem. Phys.* **2010**, *132*, 154104.
(45) Frisch, M. J.; Trucks, G. W.; Schlegel, H. B.; Scuseria, G. E.; Robb, M. A.; Cheeseman, J. R.; Scalmani, G.; Barone, V.; Petersson, G. A.; Nakatsuji, H.; Li, X.; Caricato, M.; Marenich, A.; Bloino, J.; Janesko, B. G.; Gomperts, R.; Mennucci, B.; Hratchian, H. P.; Ortiz, J. V.; Izmaylov, A. F.; Sonnenberg, J. L.; Williams-Young, D.; Ding, F.; Lipparini, F.; Egidi, F.; Goings, J.; Peng, B.; Petrone, A.; Henderson, T.; Ranasinghe, D.; Zakrzewski, V. G.; Gao, J.; Rega, N.; Zheng, G.; Liang, W.; Hada, M.; Ehara, M.; Toyota, K.; Fukuda, R.; Hasegawa, J.; Ishida, M.; Nakajima, T.; Honda, Y.; Kitao, O.; Nakai, H.; Vreven, T.; Throssell, K.; Montgomery, J. A., Jr.; Peralta, J. E.; Ogliaro, F.; Bearpark, M. J.; Heyd, J. J.; Brothers, E. N.; Kudin, K. N.; Staroverov, V. N.; Keith, T. A.; Kobayashi, R.; Normand, J.; Raghavachari, K.; Rendell, A. P.; Burant, J. C.; Iyengar, S. S.; Tomasi, J.; Cossi, M.; Millam, J. M.; Klene, M.; Adamo, C.; Cammi, R.; Ochterski, J. W.; Martin, R. L.; Morokuma, K.; Farkas, O.; Foresman, J. B.; Fox, D. J., *Gaussian 16*, Revision A.03; Gaussian, Inc.: Wallingford CT, 2017.
(46) Barrios-Rivera, J.; Xu, Y.; Wills, M. Probing the Effects of Heterocyclic Functionality in [(Benzene)Ru(TsDPENR)Cl] Catalysts for Asymmetric Transfer Hydrogenation. *Org. Lett.* **2019**, *21*, 7223−7227.

https://doi.org/10.1021/acs.organomet.1c00358
Organometallics XXXX, XXX, XXX−XXX